The Transition between Kelvin–Helmholtz and Holmboe Instability: An Investigation of the Overreflection Hypothesis

W. D. SMYTH AND W. R. PELTIER

Department of Physics, University of Toronto, Toronto, Ontario, Canada

(Manuscript received 10 July 1988, in final form 12 June 1989)

ABSTRACT

We consider the evolution of small disturbances on an inviscid, Boussinesq, stably stratified free shear layer. This flow may deliver either Kelvin–Helmholtz or Holmboe instability, depending on the details of the background stratification. Conventional one-dimensional linear analysis is employed to study the temporal and spatial structures of these instabilities and the physical mechanisms which govern their evolution. Attention is focussed upon the manner in which Kelvin–Helmholtz instability is replaced by Holmboe instability for a sequence of background flows with successively larger values of the bulk Richardson number. Unstable normal modes that exist in the transition region between the Kelvin–Helmholtz and Holmboe regimes exhibit a distinctive spatial structure, are characterized by relatively low growth rates, and are shown to occur under conditions for which overreflection of neutrally propagating internal waves apparently cannot occur because the gradient Richardson number at the steering level exceeds ¼. Detailed calculations of the propagation characteristics of internal waves in stratified shear layers reveal the extent to which resonant overreflection theory, based upon the reflection properties of temporally neutral waves, may fail to yield physical insight into the stability characteristics of such flows.

1. Introduction

A symmetric, stratified, free shear layer (i.e., one in which the shear and the stratification are distributed symmetrically about some central level) may deliver one of two types of primary instability: the Kelvin–Helmholtz instability, stationary with respect to the center of the shear layer, and the oscillatory Holmboe instability. Kelvin–Helmholtz instability has been the subject of several theoretical, experimental, and observational studies (e.g., see Klaassen and Peltier 1985, and references therein). Holmboe instability was first studied theoretically in the linear regime by Holmboe (1962), and more recently by Hazel (1972) and by Nishida and Yoshida (1984). The nonlinear behavior of Holmboe waves has been investigated in laboratory experiments [Keulegan 1949; Ellison and Turner 1959 (see description in Townsend 1958, p. 372); Thorpe 1968; Browand and Winant 1973; Maxworthy and Browand 1975; Yoshida 1977; Koop and Browand 1979; Tritton and Davies 1985; Lawrence et al. 1987] and recently by means of numerical simulation (Smyth et al. 1989, hereafter referred to as SKP).

In this paper, we shall discuss in detail the linear theory of the stability of symmetric, stratified, free shear layers, focussing upon the physical processes which govern the evolution of both Kelvin–Helmholtz and Holmboe modes. Our goal is to provide a detailed description of the influence of stratification on the stability properties of this class of flows, in order to establish a conceptual foundation in linear theory for concurrent and future nonlinear analyses, in which the somewhat exotic Holmboe waves will be explicitly related to a number of extremely interesting features of the atmospheric boundary layer which have been revealed by application of acoustic radar imaging techniques. To this end, we shall here investigate the stability characteristics of inviscid, incompressible free shear flows having the hyperbolic tangent form:

$$U(z) = \tanh z. \tag{1}$$

Of particular interest to us will be the way in which the stability characteristics of such shear layers change in the presence of symmetrically distributed stable stratification, with Brunt–Väisälä frequency given by

$$N^2(z) = J \operatorname{sech}^2 Rz, \tag{2}$$

in which R is the ratio of the length scales over which $U(z)$ and $N^2(z)$ vary and J is the value of the gradient Richardson number $\mathrm{Ri}(z) = N^2/(dU/dz)^2$ at $z = 0$. In our analyses, we shall examine the stability of the

Corresponding author address: Dr. W. R. Peltier, Department of Physics, University of Toronto, Toronto, Ontario, Canada M5S 1A7.

shear layer (1) with various stratification profiles (2), the latter being characterized by the values of the parameters R and J. Profiles (1) and (2) are illustrated in Fig. 1.

The flows described by (1) and (2) deliver two distinct forms of normal mode instability: the Kelvin–Helmholtz instability and the Holmboe instability. The former is a stationary instability (with horizontal phase speed $c_r = 0$) that also exists in the absence of stratification, while the latter is a traveling disturbance ($c_r \neq 0$) that is unstable only in stratified flows. Kelvin–Helmholtz instability occurs only in "weakly" stratified flows, i.e., flows in which J is less than some upper limit J_{KH}. The numerical value of J_{KH} depends on the detailed structure of the background flow. Holmboe instability may exist whenever $J > 0$, but for $J < J_{KH}$ Kelvin–Helmholtz modes usually have the largest growth rates. When $J > J_{KH}$, the flow may be stable, or it may exhibit Holmboe instability, depending on the form of the background profiles. Speaking broadly, then, one can state that Kelvin–Helmholtz instability is important in weakly stratified flows, while Holmboe instability is a characteristic of more strongly stratified flows (Holmboe 1962; Hazel 1972; Browand and Winant 1973). Possibly the most intriguing aspect of the behavior of these flows in the linear regime is the manner in which Kelvin–Helmholtz instability is replaced by Holmboe instability for a sequence of flows with successively higher values of J. We refer to this as the KH–Holmboe transition. In this paper, much of our attention will be focussed on the details of this transition.

In section 2, we present a detailed exposition of the stability characteristics of the inviscid, stratified, free shear layer. We describe the numerical methods used to analyze the stability of a stratified free shear layer in subsection 2a. In subsection 2b, we discuss the mathematical form of the bifurcation in the exponential growth rate that occurs as Kelvin–Helmholtz instability is replaced by Holmboe instability.

Subsection 2c is devoted to a study of the time dependence of normal mode instabilities as revealed by the dispersion relation, i.e., the dependence of the horizontal phase speed upon the wavenumber α of the disturbance and on the parameters J and R which characterize the background stratification. As we investigate the stability properties of these flows, we will encounter evidence that shows that the normal mode instabilities which the flow delivers are not always simply connected with the mechanism of internal wave overreflection. (The reader will find a detailed recent review of the application of the overreflection idea to the understanding of instability in Lindzen 1988). In particular, we will find unstable modes in the vicinity of the KH–Holmboe transition whose associated neutral waves have critical levels in regions of the flow at which the gradient Richardson number exceeds ¼, a circumstance in which overreflection cannot occur (Booker and Bretherton 1967; Jones 1968; Lindzen and Barker 1985). This anomaly is investigated further in section 3.

In subsection 2d we examine the spatial structures of the Kelvin–Helmholtz and Holmboe instabilities and the physical mechanisms that govern their evolution. By examining profiles of the Reynolds stress and the vertical energy flux, we will see that unstable modes in the vicinity of the KH–Holmboe transition are configured in a somewhat unusual way. This configuration may account for the low growth rates exhibited by instabilities occurring near the KH–Holmboe transition.

Section 3 is devoted to the application of resonant overreflection theory to the prediction of the stability characteristics of stratified shear layers. In subsection 3a, we examine profiles of the vertical energy flux for neutrally propagating internal waves, in order to determine whether such waves are overreflected. We confirm that unstable normal modes whose critical levels are located in regions where the Richardson number exceeds ¼ are not described by the overreflection of contiguous neutral waves. Finally, we present the results of explicit calculations of wave propagation characteristics in which we attempt to identify unstable normal modes with overreflected neutral waves over a broad region of parameter space. The methodology and results of this study are described in subsections 3b and 3c, respectively. In section 3d, we examine the consistency condition employed by Lindzen and Rosenthal (1983) in order to correct discrepancies between the predictions of overreflection theory and those of linear stability analysis. We show analytically that this consistency condition is equivalent to the matching condition which identifies normal modes in the stability problem. The physical interpretation of these results is discussed in section 4.

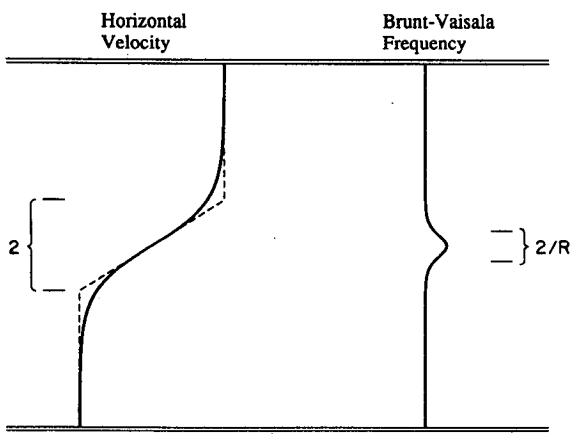

FIG. 1. Solid curves represent the profiles of background velocity and stratification given by (1) and (2) for the case $R = 3$. The dashed curve illustrates the piecewise-linear velocity profile which is employed in the quantitative overreflection calculations.

2. Linear stability analysis

In this section, we examine the spatial structure and temporal evolution of Kelvin–Helmholtz and Holmboe instabilities using conventional linear stability analysis, beginning with a brief exposition of the methods employed.

a. Methodology

We perform the normal-mode stability analysis for a stratified free shear layer using a parallel shooting method similar to that employed by Hazel (1972). The relevant stability equation in the Boussinesq limit is the Taylor–Goldstein equation (e.g., Miles 1961)

$$\frac{d^2\psi'}{dz^2} + \left[\frac{N^2}{(U-c)^2} - \frac{d^2U/dz^2}{U-c} - \alpha^2\right]\psi' = 0, \quad (3)$$

in which ψ' is the z-dependent amplitude of the perturbation streamfunction, c is the complex phase speed, α the horizontal wavenumber of the wave, and U and N^2 the profiles of background velocity (1) and Brunt–Väisälä frequency (2), respectively. All quantities are nondimensionalized using the half-width of the shear layer as the length scale and the background velocity at $z \to +\infty$ as the velocity scale.

Equation (3) is solved subject to the condition that the dependent variable $\psi'(z)$ remains bounded for all z. Far away from the shear layer, (3) has solutions $\psi' \sim e^{\pm\alpha z}$, and we satisfy the boundedness condition by choosing the appropriate sign for the exponent. The boundedness condition is easily shown to be equivalent to a condition of outgoing radiation. This equivalence will be important in section 3, where we examine the propagation characteristics of neutral disturbances.

Together with the boundedness condition, (3) constitutes a linear eigenvalue problem that implicitly defines a dispersion relation $c = c(\alpha)$ for a given background flow. Often we will be interested not in the phase speed $\mathrm{Re}(c)$ but in the exponential growth rate $\sigma = \alpha\,\mathrm{Im}(c)$.

It can be shown from the symmetry of the eigenvalue problem that if c is an eigenvalue, then its complex conjugate is also an eigenvalue (e.g., Hazel 1972), i.e., every decaying mode is accompanied by a growing mode, so we need only consider values of c lying in the upper half-plane. In addition, the semicircle theorem (Howard 1961) assures us that such eigenvalues must lie within the unit circle $|c| < 1$. Having established these limits on the value of c for an unstable mode, we can now locate, for a given α, all of the roots c of the matching function $M(c, \alpha)$ and thus compute the dispersion relation $c = c(\alpha)$. The numerical integration of (3) is performed using the recently devised ODE solver ERNY (Sharp and Fine 1987), which is based on a Runge–Kutta–Nystrom formula pair. Roots of the matching function are found using a quadratic interpolation scheme based on Muller's method (Muller 1956) in combination with contour plots of the matching function, which are employed to ensure that all of the roots have indeed been found.

Once we have found a set of eigenvalues c and α, we may examine the corresponding eigenfunction $\psi'(z)$, as well as the eigenfunctions for vertical and horizontal velocity, potential temperature (or density) and pressure, and the vertical fluxes of momentum, energy and heat that are affected by the disturbance.

b. The KH–Holmboe transition

As was mentioned in the Introduction, a major point of interest in our new linear analyses of stratified free shear flows will be the transition from Kelvin–Helmholtz instability to Holmboe instability as the bulk Richardson number J is increased through the critical value J_{KH}. In this section, we will examine the nature of this transition.

We plot in Fig. 2 the real and imaginary parts of the exponential growth rate σ of a normal mode disturbance with $\alpha = 0.3$ on a background flow with scale ratio $R = 8$ and with bulk Richardson number increasing from 0 to 1. When J is close to zero, a single unstable mode exists. This mode is stationary with respect to the center of the shear layer, as its growth rate is purely real, and it is thus identified as a Kelvin–Helmholtz instability. The growth rate of the Kelvin–Helmholtz mode decreases with increasing J, as one would expect in consequence of the stabilizing effect of the stratification. Near $J = 0.15$, however, a second Kelvin–Helmholtz mode is destabilized, whose growth rate increases with increasing J. When J reaches the critical value 0.43, the growth rates of the two Kelvin–Helmholtz modes become equal. Beyond this point, the two modes retain a common value of σ_r (solid curves) that decreases slowly with increasing J, and they acquire distinct nonzero values of σ_i (dashed curves). Thus we see that the character of the instability has changed from stationary ($\sigma_i = 0$) to oscillatory ($\sigma_i \neq 0$), i.e., that Holmboe instability has appeared. Note that the two values of σ_i in the Holmboe branch are equal in magnitude but opposite in sign, meaning that if the amplitudes of the two modes were equal, they would interfere to create a simple standing wave.

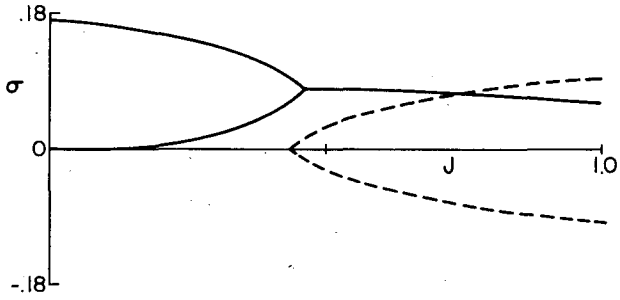

FIG. 2. Growth rate versus stratification for shear layer with $R = 8$, $\alpha = 0.3$. The solid curve represents the real part of σ whereas the dashed curve denotes the imaginary part of σ.

c. Dispersion relations

In Fig. 3, we plot $\sigma(\alpha)$ for four background flows, which consist of hyperbolic tangent shear layers (1) with stratification profiles (2) characterized by the parameter values $R = 8$ and $J = 0$, 0.2, 0.4 and 0.6, respectively. Figure 3a illustrates the unstratified case, with $J = 0$. Only Kelvin–Helmholtz (Rayleigh) instability is present, and the fastest-growing mode is located at $\alpha = 0.45$. In Fig. 3b, moderate stratification has been introduced ($J = 0.2$), and we find Holmboe instability when $\alpha > 0.5$, but the fastest-growing mode is the Kelvin–Helmholtz instability at $\alpha = 0.35$. In Fig. 3c, J has been increased to 0.4. We now find Kelvin–Helmholtz and Holmboe modes with comparable growth rates, but Kelvin–Helmholtz instability still dominates, with the growth rate maximized at $\alpha = 0.3$. When J is increased to 0.6 (Fig. 3d), we find that Kelvin–Helmholtz instability is no longer present, and the fastest-growing instability is the Holmboe mode at $\alpha = 0.6$.

A broader view of the stability characteristics of these flows may be gained by investigating σ as a function of the three parameters α, J and R. We do this by taking slices R = constant through (α, J, R) space and plotting contours of equal σ_r and equal σ_i on the remaining (α, J) planes. Four such plots are shown in Fig. 4, corresponding to the cases $R = 8$, $R = 3$, $R = 2.4$ and $R = 1$. [The corresponding diagram for the single case $R = 5$ is given in Hazel (1972).] Note that Figs. 2 and 3a–d are essentially cross sections of Fig. 4a, although the contour plots in Fig. 4 show only the fastest-growing mode at each point in the α–J plane, and only the mode with $\sigma_i > 0$ in the case of a complex conjugate eigenvalue pair.

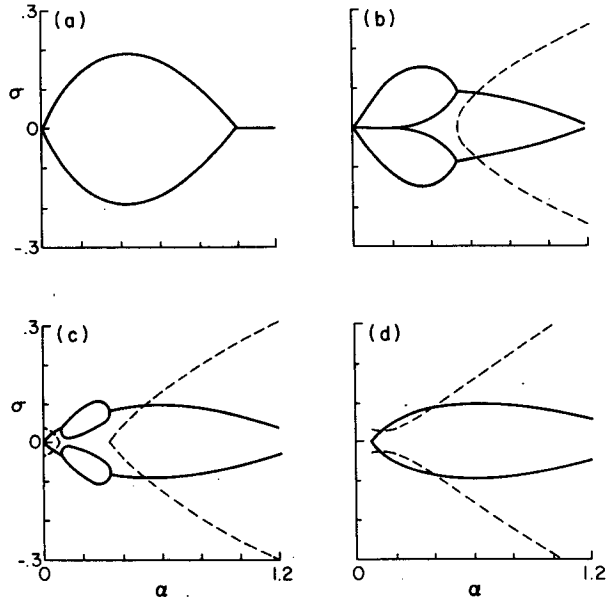

FIG. 3. Growth rate versus wavenumber for stratified shear layer with $R = 8$ and (a) $J = 0$, (b) $J = 0.2$, (c) $J = 0.4$ and (d) $J = 0.6$. The solid curves denote the real part of σ, the dashed curves the imaginary part of σ.

It will be apparent upon inspection of Fig. 4 that the domain of instability ($\sigma_r \neq 0$) extends to very large values of J in the cases $R = 8$, $R = 3$ and $R = 2.4$, but is limited to $J < \frac{1}{4}$ in the case $R = 1$. The Miles–Howard theorem (Miles 1961; Howard 1961) demonstrates that a flow is stable unless the gradient Richardson number $\mathrm{Ri}(z) = N^2/(dU/dz)^2$ is less than $\frac{1}{4}$ for some z. This result may be applied to the profiles (1) and (2) (Hazel 1972; SKP) to show that the existence of instability at large values of J depends crucially upon the value of R. Specifically, it may be shown that (i) when $R < \sqrt{2}$, J represents the minimum value of the gradient Richardson number $\mathrm{Ri}(z)$, and hence instability is possible only when $J < \frac{1}{4}$; (ii) when $\sqrt{2} < R < 2$, a maximum value of J (exceeding $\frac{1}{4}$) exists, above which instability cannot occur; and (iii) when $R > 2$, the flow may be unstable at any value of J. Since Ri approaches zero far from the shear layer for all z, profiles of $\mathrm{Ri}(z)$ for various R are shown in Hazel (1972). The Miles–Howard theorem does not guarantee the existence of instability in any of these flows (or in any flow); only an explicit linear stability analysis can determine whether or not a given flow in which $\mathrm{Ri}(z) < \frac{1}{4}$ for some z actually becomes unstable. We have constructed contour plots of $\sigma(\alpha, J)$ for many values of R, and have found that $R = 2.4$ represents an approximate lower limit on the range of R for which instability exists for all values of J.

A very important feature of the $\sigma(\alpha, J)$ diagrams presented in Fig. 4 is the contour $\sigma_i = 0$, which marks the transition between Kelvin–Helmholtz instability and Holmboe instability. In the case $R = 1$ (Fig. 4d), this transition does not occur; only Kelvin–Helmholtz modes are unstable. At the larger values of R (Figs. 4a–c), Holmboe instability is present for all J, and becomes dominant at large J, where Kelvin–Helmholtz modes are stabilized by the intense stratification. It must be noted that each unstable Holmboe mode shown in Figs. 4a–c actually represents a pair of complex conjugate modes, i.e., modes with equal growth rates and equal but oppositely directed horizontal phase speeds. Each Holmboe instability may in fact be considered to consist of the superposition of such a mode pair, and this gives the instability its standing wavelike character in a typical numerical simulation (SKP). This aspect of Holmboe instability will be discussed further in section 2d, where we shall examine the spatial structures of both the Kelvin–Helmholtz and Holmboe modes.

In Figs. 4a, 4b and 4c, there are substantial regions of parameter space in which growth rates of normal modes increase with increasing stratification, i.e., $\partial\sigma_r/\partial J > 0$. This is not surprising, since we know that Holmboe instability depends on the stratification for its existence, but it raises the possibility that the fastest-

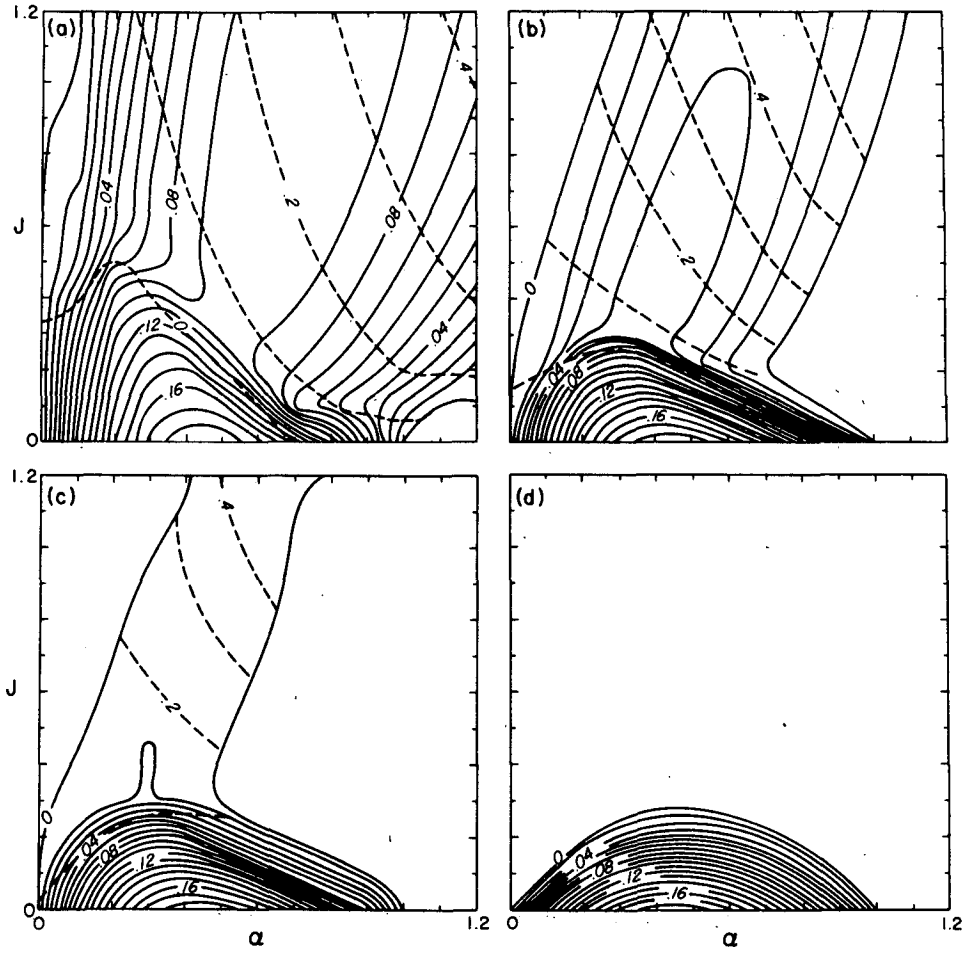

FIG. 4. Contour plots of growth rate versus wavenumber and bulk Richardson number for (a) $R = 8$, (b) $R = 3$, (c) $R = 2.4$ and (d) $R = 1$. Solid and dashed curves represent contours of the real and imaginary parts, respectively.

growing modes of instability at some points in parameter space might be three-dimensional, i.e., their properties may vary with the spanwise coordinate y (Yih 1955; Lawrence et al. 1987). Detailed calculations (SKP) have revealed, however, that this does not occur in any of the inviscid model flows considered here, and we are thus justified in restricting our attention to two-dimensional disturbances.

Figures 4a and 4b immediately reveal the existence of unstable normal modes whose growth is apparently not illuminated by consideration of internal wave overreflection. This may be seen most easily by considering the Kelvin–Helmholtz modes. Because these modes are stationary, their associated critical levels [values of z at which $U(z) = c_r$] are located at the center of the shear layer ($z = 0$) and hence the value of the gradient Richardson number at the critical level, Ri_c, is equal to the bulk Richardson number J. Overreflection cannot occur unless $\mathrm{Ri}_c < \frac{1}{4}$ (Jones 1968; Davis and Peltier 1977; Lindzen and Barker 1985) yet we see in Figs. 4a and 4b regions in which Kelvin–Helmholtz instability exists for J substantially greater than ¼. In addition, on the opposite side of the KH–Holmboe transition at $\sigma_i = 0$, Holmboe modes exist whose associated critical levels are located inside the region surrounding $z = 0$ within which $\mathrm{Ri}(z) > \frac{1}{4}$, and therefore these modes apparently cannot be understood by consideration of the overreflection mechanism either. In later sections of this paper, we will verify explicitly that the neutral modes associated with unstable modes for which $\mathrm{Ri}_c > \frac{1}{4}$ (in the sense that they have the same phase speed as these modes) are not overreflected. As we will point out, however, the expectation that there should be such an association may be unwarranted.

d. Eigenfunctions of the normal modes

In the previous subsection we examined the rate of temporal growth of unstable normal modes as described by the dispersion relation. In this section we

will employ profiles of the eigenfunctions of the Taylor–Goldstein equation (3), and related functions, to reveal the spatial structures and growth mechanisms of these modes.

Specifically, we will examine the z-dependent parts of the complex eigenfunctions for vertical velocity, horizontal velocity, pressure and potential temperature. In addition, we will plot the correlations $\overline{u'w'}$, $\overline{p'w'}$, $\overline{\theta'w'}$ and $\frac{1}{2}(\overline{u'u'} + \overline{w'w'})$, which appear in the following height-dependent energy equation for small disturbances on an inviscid stratified shear flow:

$$\frac{1}{2}\frac{\partial}{\partial t}\{\overline{u'u'} + \overline{w'w'}\} = -\frac{dU}{dz}\overline{u'w'} - \frac{\partial}{\partial z}\overline{p'w'} + J\overline{\theta'w'}. \tag{4}$$

In this equation, the processes governing the evolution of the perturbation kinetic energy profile are represented by a sum of three terms. On the right-hand side of (4) these are respectively the Reynolds stress term, which describes the transfer of kinetic energy between the background flow and the perturbation, the flux divergence term, which represents a contribution from the vertical flux of perturbation kinetic energy, and the heat flux term, which describes the conversion between perturbation kinetic energy and potential energy.

Figure 5 displays plots of the eigenfunctions and the above-mentioned correlations for a Kelvin–Helmholtz mode with $\alpha = 0.3$, growing on a hyperbolic tangent shear layer with stratification parameters $J = 0.01$ and $R = 3$. When the background shear $dU(z)/dz$ and the Brunt–Väisälä frequency $N^2(z)$ are symmetric about $z = 0$, as is the case in the present study, the symmetry of the Taylor–Goldstein equation dictates that every growing mode with phase velocity c must be accompanied by a decaying mode with phase velocity c^*. Figure 6 shows the eigenfunctions and correlations for the decaying mode which corresponds in this way to the growing mode illustrated in Fig. 5. The Kelvin–Helmholtz modes illustrated in Figs. 5 and 6 have relatively simple spatial structures. We will discuss these modes in detail in order to establish the manner in which the eigenfunctions and correlations are to be interpreted. We will discuss first the similarities and then the differences between Figs. 5 and 6. Following this, we will go on to examine Holmboe modes and modes lying near the KH–Holmboe transition, whose spatial structures and growth mechanisms are more complex.

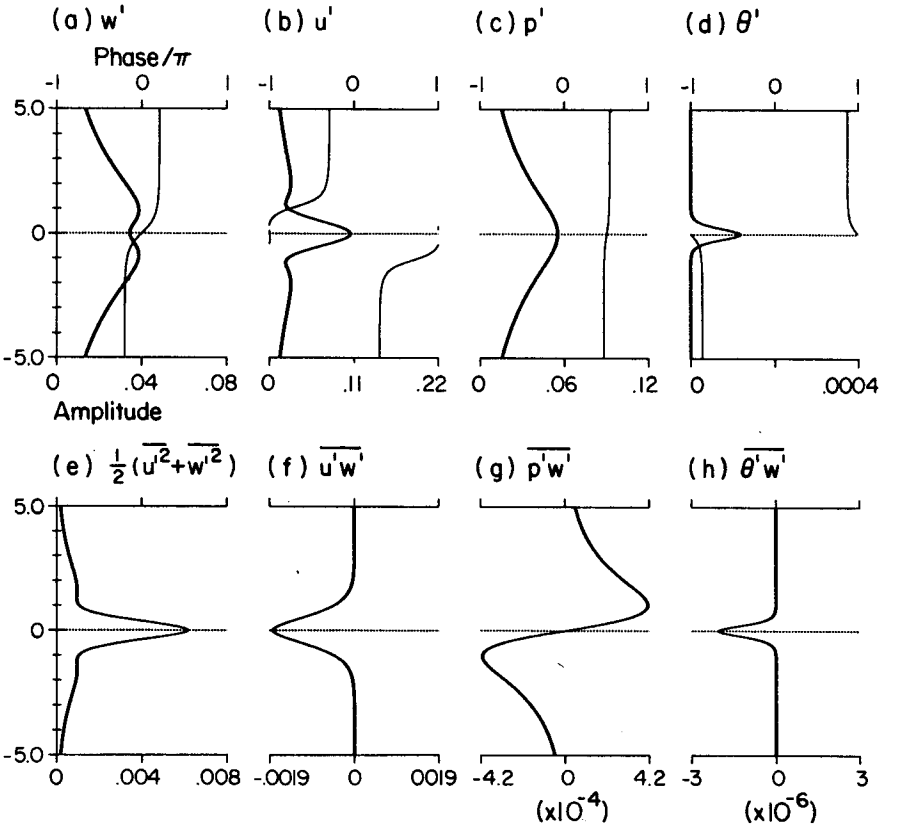

FIG. 5. Eigenfunctions and correlations for the growing Kelvin–Helmholtz mode with $R = 8$, $J = 0.01$, $\alpha = 0.3$ and $c_i = 0.1719$. Dark (light) curves represent amplitude (phase). Horizontal dotted line indicates critical level of corresponding neutral wave.

The following observations pertain to both Figs. 5 and 6:

(i) When $c_r = 0$, the Taylor–Goldstein equation is symmetric about $z = 0$, and this symmetry is evident in the solutions. We will see that this symmetry is broken when $c_r \neq 0$, i.e., for Holmboe modes.

(ii) The horizontal velocity u' is considerably greater in magnitude than the vertical velocity w', and is concentrated in a narrow jet surrounding $z = 0$.

(iii) The potential temperature perturbation is concentrated near $z = 0$, due to the strong gradient of the background potential temperature profile in that region.

The remaining observations concern contrasts between the growing mode shown in Fig. 5 and the decaying mode shown in Fig. 6:

(iv) The growing mode is characterized by a negative correlation between the perturbation horizontal and vertical velocities, i.e., $\overline{u'w'} < 0$. This may be interpreted to mean that the disturbance works to reduce the background shear by inducing a net downward flux of horizontal momentum. As the background shear is reduced, so is the kinetic energy that it contains, and energy conservation then dictates that the disturbance must grow. In contrast, the decaying mode shown in Fig. 6 is characterized by $\overline{u'w'} > 0$. This relationship between the sign of $\overline{u'w'}$ and the direction of energy transfer between the disturbance and the background flow is also evident in the Reynolds stress term in (4).

(v) The direction of the energy transfer between the disturbance and the background flow is also revealed by the tilt in the phase of the eigenfunction w', which is opposite to the tilt in the streamlines for a normal mode disturbance. It is easily verified that if $w' = r(z)\exp(i\phi(z))$, $r(z)$ and $\phi(z)$ being real-valued functions, then

$$\overline{u'w'} = -\frac{1}{2\alpha} r^2 \frac{d\phi}{dz}, \tag{5}$$

and thus $d\phi/dz > 0$ implies that $\overline{u'w'} < 0$. This connection between the tilt of the streamlines and the direction of the energy transfer is strongly suggestive of the operation of the "Orr" mechanism (see Lindzen 1988 for a recent discussion). Klaassen and Peltier (1985) have shown that as the Kelvin–Helmholtz instability grows beyond the linear regime, nonlinearity tends to reduce the tilt of the perturbation streamlines, and that wave growth stops (i.e., the wave reaches its maximum amplitude) when the streamlines become vertical.

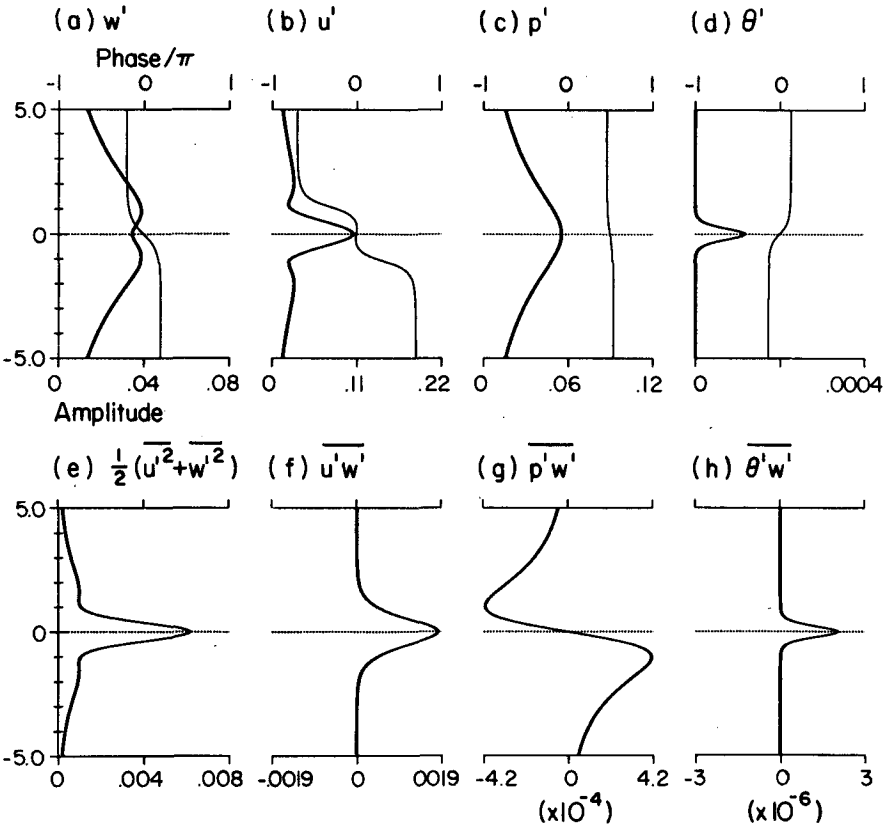

FIG. 6. Eigenfunctions and correlations for decaying Kelvin–Helmholtz mode. Parameter values as in Fig. 5, except $c_i = -0.1719$.

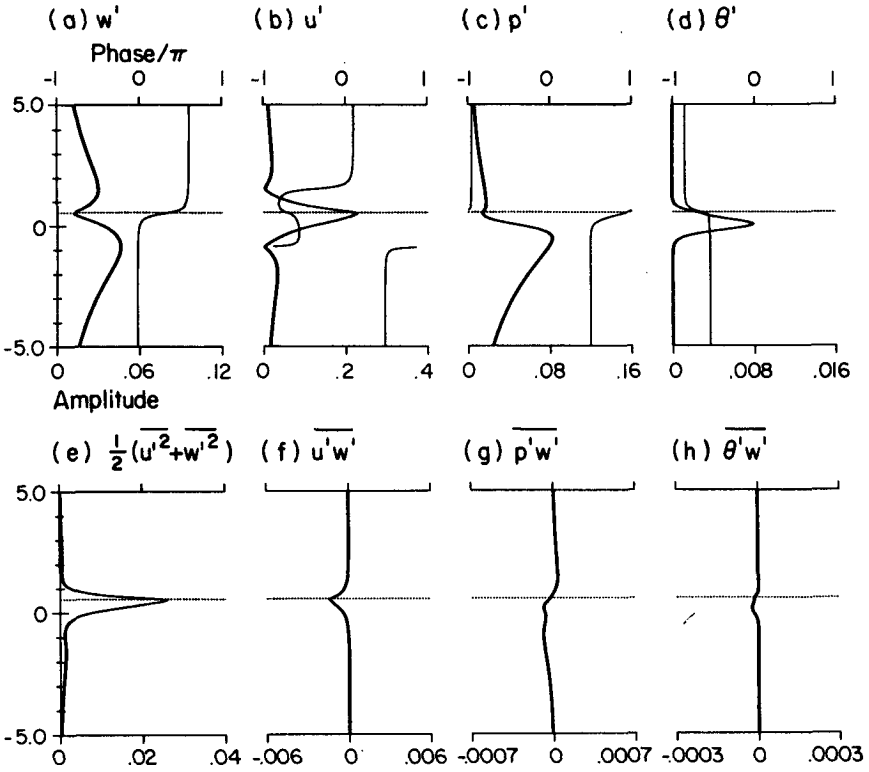

FIG. 7. Eigenfunctions and correlations for right-moving Holmboe mode with $R = 3$, $J = 0.6$, $\alpha = 0.3$, $c_r = 0.5055$, and $c_i = 0.0833$.

(vi) The correlation $\overline{p'w'}$ represents a vertical flux of perturbation kinetic energy, as may be seen by inspection of the flux divergence term in (4). If $\overline{p'w'} > 0$ at some point, the net vertical energy flux due to the disturbance at that point is directed upward, while the reverse is true if $\overline{p'w'} < 0$. As was noted under observation (iv), the fact that $\overline{u'w'} < 0$ for the growing mode shown in Fig. 5 indicates that perturbation energy is "created" (i.e., extracted from the background flow) in the vicinity of the shear layer. Thus, we are not surprised to find that this region acts as an energy source, i.e., that perturbation energy flows out from the shear layer to the other regions of the flow. In Fig. 6, we observe the opposite process; perturbation energy flows into the shear layer, where it is transferred via the Reynolds stress to the background flow.

(vii) The vertical flux of heat due to the disturbance is given by the correlation $\overline{\theta'w'}$. In Fig. 5h, we see that $\overline{\theta'w'} < 0$ for the growing Kelvin–Helmholtz mode. The disturbance works to reduce the ambient potential temperature gradient by inducing a net downward flux of heat (or an upward flux of mass). Thus, a part of the kinetic energy extracted from the background shear is used to increase the gravitational potential energy of the flow. In contrast, the decaying mode shown in Fig. 6 acts to increase the ambient potential temperature gradient, thus decreasing the potential energy of the flow, and passes that energy (along with its own initial energy) back into the background flow in the form of kinetic energy, i.e., as an increase in the background shear. This illustrates the results of Klaassen and Peltier (1985) regarding the energy budget in a stratified shear flow and the direction of energy transfers between the potential, mean flow kinetic, and wave kinetic energy reservoirs.

In Fig. 7, we show the eigenfunctions and correlations for a Holmboe mode with $\alpha = 0.3$ growing on a strongly stratified hyperbolic tangent shear layer with $J = 0.6$ and $R = 3$. In addition to the presence of a corresponding decaying mode, the symmetry of the Taylor–Goldstein equation (3) requires that each growing mode with phase speed c be accompanied by a second growing mode with phase speed $-c^*$. When $c_r = 0$, as was the case with the Kelvin–Helmholtz modes shown in Figs. 5 and 6, there is no difference between these modes. In the present case, however, we have $c = 0.505467 + 0.083320i$, so that a second growing mode with $c = -0.505467 + 0.083320i$ must exist. The eigenfunctions and correlations of the latter mode are illustrated in Fig. 8. The disturbance shown in Fig. 7 is right-moving, i.e., $c_r > 0$, while the disturbance shown in Fig. 8 is left-moving.

We notice immediately that the symmetry about $z = 0$ which was evident in Figs. 5 and 6 has been broken. This is because there is now, in addition to $z = 0$, a second level which is important in the evolution of the

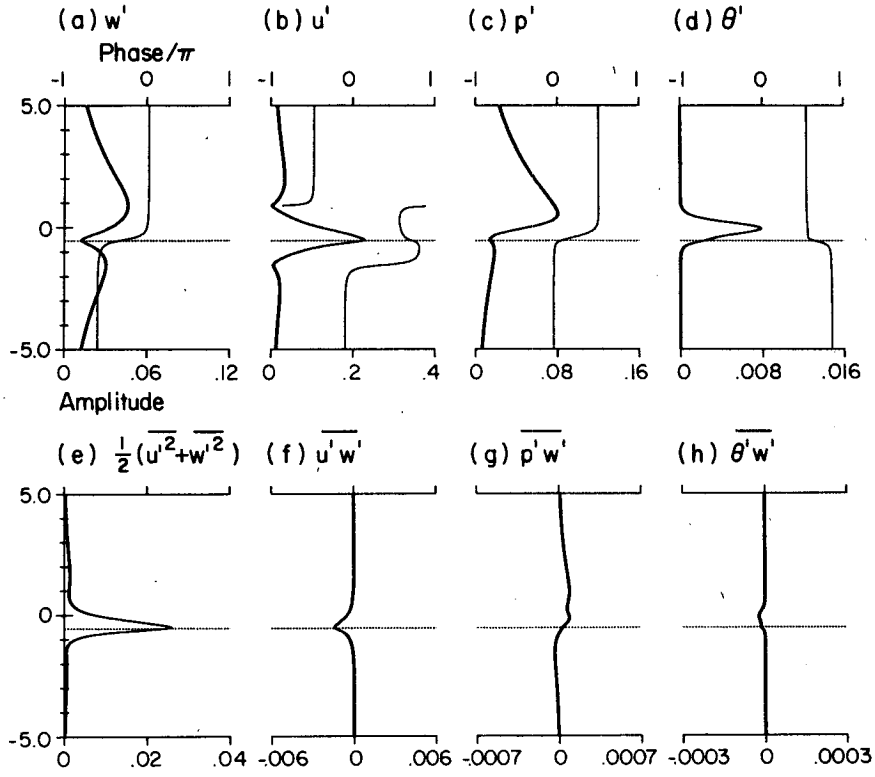

FIG. 8. Left-moving Holmboe mode; parameter values as in Fig. 7, except $c_r = -0.5055$.

mode, namely the steering level or the critical level of the associated neutral mode (see section 3), which we call z_c. In Figs. 5 and 6, $z_c = 0$, so that symmetry about $z = 0$ is preserved, but in this case $z_c = \pm 0.5566$, with the right-going mode having its steering level in the upper region of the shear layer and the left-going mode having its steering level in the lower region. Figures 7f and 8f show that $\overline{u'w'}$ is a minimum at $z = z_c$, i.e., that this is the level at which the disturbance is optimally configured to draw energy from the background shear, while Figs. 7e and 8e reveal that the kinetic energy of each mode is concentrated near $z = z_c$. Furthermore, the $\overline{p'w'}$ plots (Figs. 7g and 8g) show that the critical level acts as a source of energy for the disturbance. Comparison of the maximum amplitudes of u' and w' shows that the dominance of horizontal motion over vertical motion is more pronounced than it was in the weakly stratified case (cf., Fig. 5).

The two modes illustrated in Figs. 7 and 8 are qualitatively very similar to Kelvin–Helmholtz modes; however, the fact that their exponential growth rates σ_r are identical implies that if that common growth rate represents the global maximum of $\sigma_r(\alpha)$ for a given background flow, then the fastest-growing instability for that flow must be defined as the superposition of the two individual modes. For simplicity, we take the amplitudes of the component modes to be equal, and we refer to that superposition as the Holmboe instability.[1] The eigenfunctions of the two modes are related by the inversion operation $f(z) \rightarrow f^*(-z)$ (Hazel 1972), so that their amplitudes are equal at $z = 0$. Thus the superposition of the two modes creates, near the center of the shear layer, the effect of a standing wave. In the upper part of the shear layer, the superposition is dominated by the right-going mode, while the left-going mode dominates in the lower region. This superposition determines the oscillatory structure of the Holmboe wave, which has been the subject of several laboratory experiments (see references given in the Introduction), and which has recently been investigated by means of nonlinear numerical simulation (SKP).

In Figs. 9 and 10, we illustrate the evolution of the Holmboe instability through one half-cycle by plotting the eigenfunctions (Fig. 9) and the correlations (Fig. 10) of the superposition of the two component modes

[1] While the probability of the initial amplitudes being exactly equal in a physical flow is zero, results from nonlinear numerical simulations (in progress) and from laboratory experiments (e.g., Lawrence et al. 1987; Maxworthy and Browand 1975) indicate that the qualitative behavior of the Holmboe wave is not strongly dependent upon the equality of these two amplitudes. The special case in which the two amplitudes are equal is thus an interesting special case to study, and is the logical starting point for the study of the more general case in which an asymmetry of amplitudes exists.

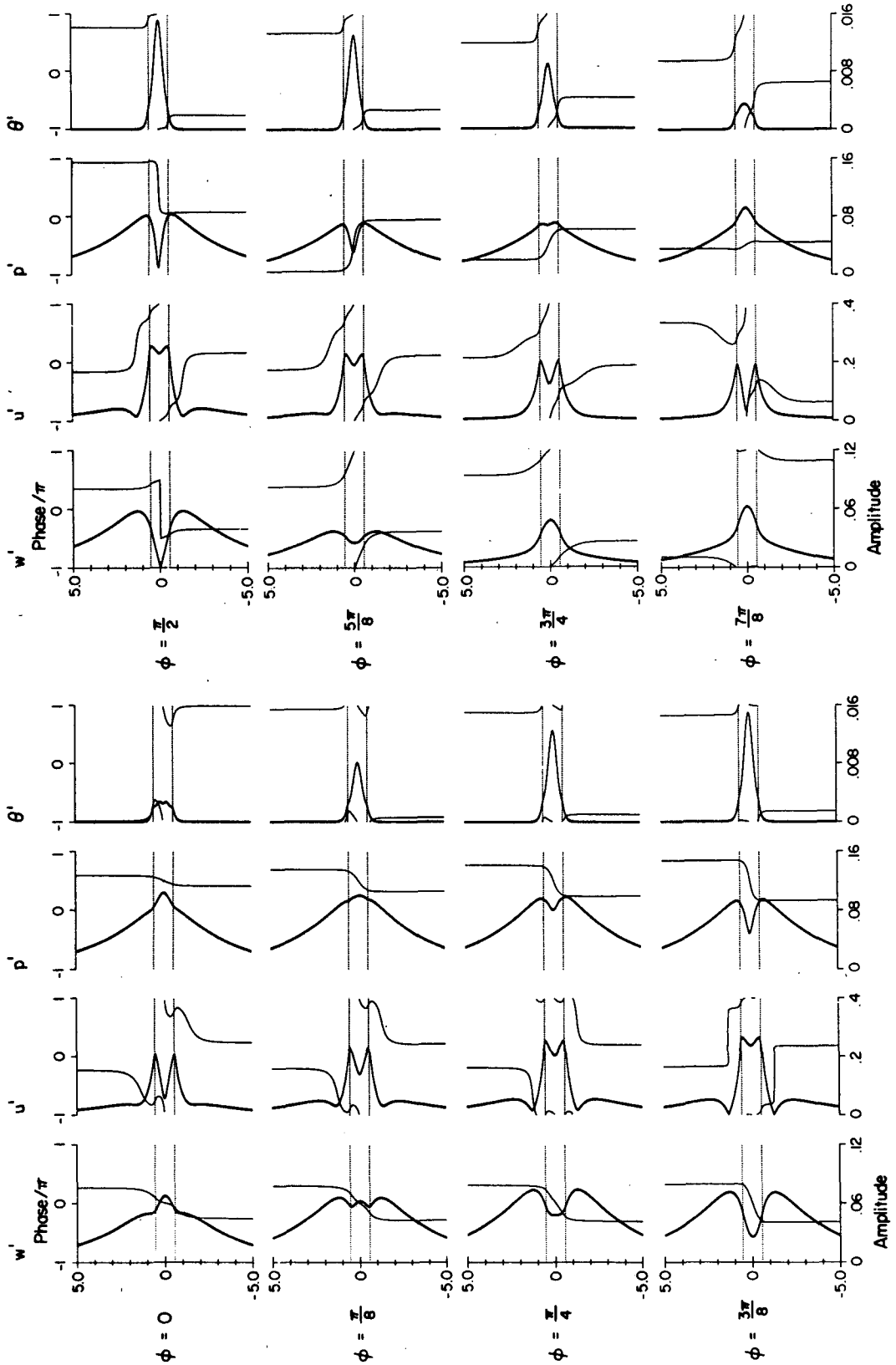

FIG. 9. Eigenfunctions for Holmboe instability consisting of a superposition of the modes shown in Figs. 7 and 8, evolving through one half-oscillation. Exponential growth is suppressed.

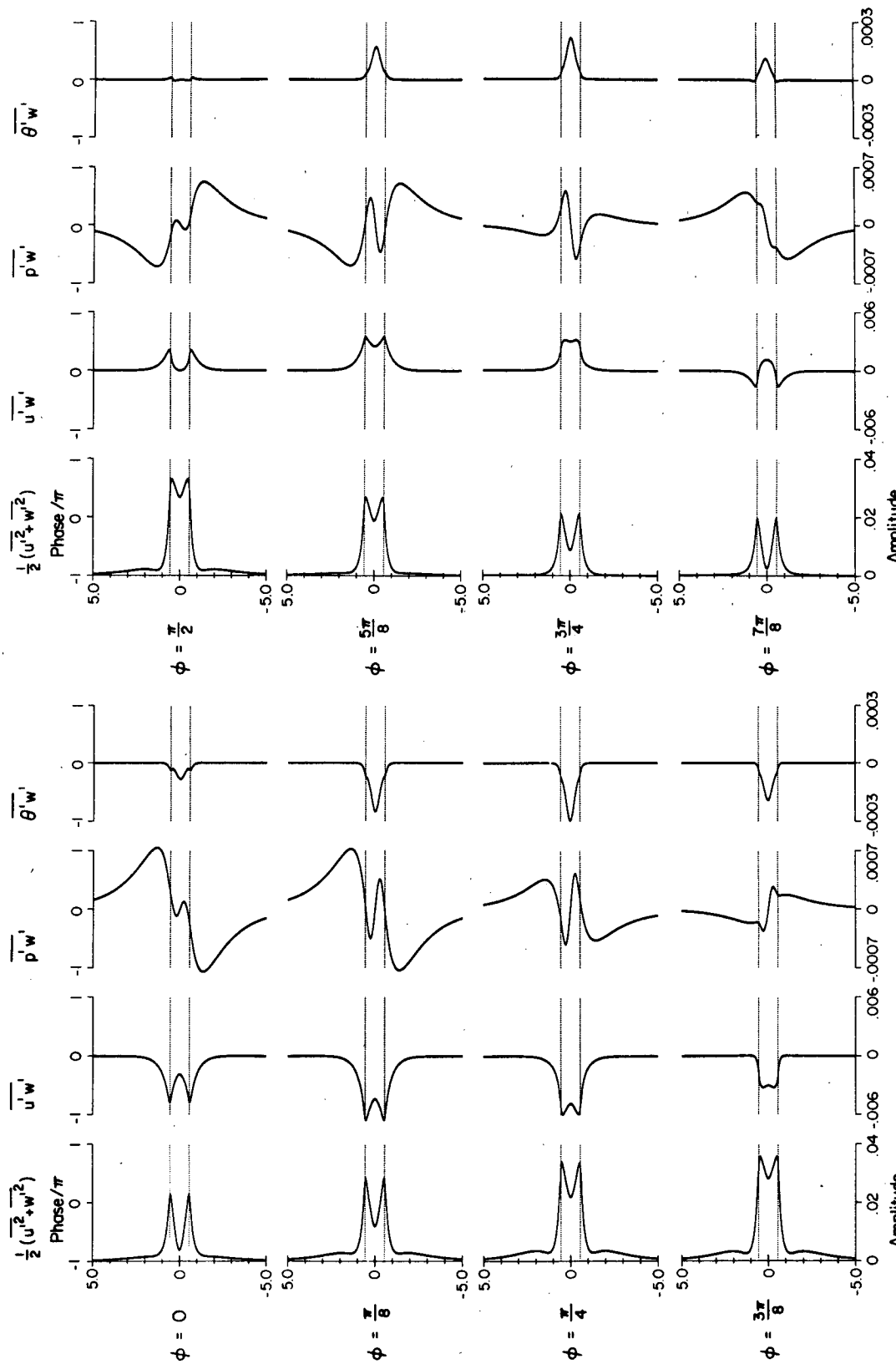

FIG. 10. Correlations for Holmboe instability consisting of a superposition of the modes shown in Figs. 7 and 8, evolving through one half-oscillation. Exponential growth is suppressed.

at points in the oscillation cycle separated by a phase change $\Delta\phi = \pi/8$. These changes in phase occur in the factor $e^{-i\alpha c_r t}$, which describes oscillatory time dependence in a normal mode, i.e., $\Delta\phi = -\alpha c_r \Delta t$. The exponential growth factor $e^{\alpha c_i t}$ has been suppressed. We illustrate only the first half of the cycle, from $\phi = 0$ to $\phi = \pi$. The second half of the cycle, from $\phi = \pi$ to $\phi = 2\pi$, is identical to the first half except for a phase shift $e^{i\pi}$ (i.e., a sign change) in the eigenfunctions. As the oscillatory behavior of the Holmboe instability is somewhat complex, we will describe the evolution of each eigenfunction and correlation through the half-cycle in sequence, adding to the numbered list of observations which we began earlier in this subsection.

(vii) At $\phi = 0$, the phase tilt of the vertical velocity eigenfunction w' of the Holmboe instability is positive, indicating growth [see observation (v)]. As ϕ changes from 0 to $\pi/2$, the amplitude of w' at $z = 0$ drops continuously to zero. At $\phi = \pi/2$, the phase of w' shifts at $z = 0$. Beyond this point in the cycle, $|w'|$ at $z = 0$ becomes nonzero again, but the phase tilt now indicates that the disturbance is decaying.

(ix) The horizontal velocity eigenfunction u' is characterized by peaks in amplitude at the steering levels. The existence of horizontal jets in the perturbation flow field near steering levels is a common feature of shear flow instabilities [see observation (ii) and Figs. 5–8].

(x) Like the phase tilt in w', the correlation $\overline{u'w'}$ reveals that the disturbance grows when $0 < \phi < \pi/2$ and decays when $\pi/2 < \phi < \pi$, whereupon the pattern is repeated.

(xi) The most obvious feature of the energy flux profile is that the sign of $d(\overline{p'w'})/dz$ at $z = 0$ generally differs from the sign of the net change in $\overline{p'w'}$ across the shear layer (from $z = -1$ to $z = +1$, say). The net change in $\overline{p'w'}$ across the shear layer behaves as one would expect; it indicates that the shear layer acts as a source of energy for the disturbance [see observation (vi)] in those parts of the cycle during which the disturbance is growing, and as a sink when the disturbance is decaying. Near $z = 0$, however, the opposite result is found.

(xii) The heat flux profile $\overline{\theta'w'}$ behaves very much like the correlation $\overline{u'w'}$. During the growth phase of the cycle, a portion of the energy which the disturbance extracts from the background flow is channeled into the potential energy reservoir via the negative heat flux, as was found for the growing wave illustrated in Fig. 5. In the decay phase, the disturbance returns a part of this potential energy to the background kinetic energy reservoir. This behavior has been previously noted in connection with the interpretation of nonlinear Holmboe wave simulations (SKP).

The most significant result illustrated in Figs. 9 and 10 is that the exponential growth of the Holmboe instability is modulated by a periodic oscillation due to changes in the phase relationship between the left- and right-moving modes that combine to form the instability. This behavior was first predicted by Holmboe (1962) using his "method of symmetric waves," and was verified numerically by SKP.

We have examined the spatial structure of a Kelvin–Helmholtz instability growing on a weakly stratified flow and that of a Holmboe instability growing on a strongly stratified flow. We now turn our attention to the transition region between Kelvin–Helmholtz and Holmboe instability. In Fig. 11, we show the eigenfunctions and correlations for a Kelvin–Helmholtz mode with $\alpha = 0.3$, on a background flow with stratification parameters $R = 3$ and $J = 0.26$. This is very close to the KH–Holmboe transition for these values of R and α, which is located at $J_{KH} = 0.261$.

An important feature to note in Fig. 11 is the z-dependence of the perturbation energy flux (Fig. 11g) near $z = 0$. We see that a "kink" (i.e., a reversal in slope) has developed in $\overline{p'w'}$ near $z = 0$ which did not appear in the weakly stratified case (cf., Fig. 5g). The presence of this kink near $z = 0$ implies that the region surrounding the steering level acts as an energy sink for the disturbance, even though the extraction of energy from the mean flow takes place almost entirely in this region, as can be seen from the $\overline{u'w'}$ profile in Fig. 11f. [Note in addition that the Reynolds stress term in (13), which describes the transfer of energy to and from the mean flow, includes the factor $dU/dz = \mathrm{sech}^2 z$, which concentrates the region of energy extraction even further.]

As J is increased from zero to approach the transition value J_{KH}, a second Kelvin–Helmholtz mode is destabilized (see Fig. 2). The growth rate σ_r of the second mode increases with increasing J and becomes equal to the growth rate of the faster-growing mode when $J = J_{KH}$. Shown in Fig. 12 are the eigenfunctions and correlations for the second Kelvin–Helmholtz mode that exists at $R = 3$, $J = 0.26$, $\alpha = 0.3$. The growth rate of the second mode is $\sigma_r = 0.0245$, while the growth rate of the mode illustrated in Fig. 11 is $\sigma_r = 0.0401$. The physical structures of the two modes differ in detail only. The eigenfunctions of the slower-growing mode undergo sharper phase shifts at the steering level than do those of the faster-growing mode shown in Fig. 11, and the correlations $\frac{1}{2}(\overline{u'u'} + \overline{w'w'})$, $\overline{u'w'}$ and $\overline{\theta'w'}$ are more strongly concentrated near the steering level.

We now show that the existence of an energy sink surrounding the steering level is a characteristic of modes for which the gradient Richardson number at the steering level exceeds ¼. Figure 13 contains the $\overline{p'w'}$ profiles for a sequence of unstable modes with $\alpha = 0.3$, growing on background flows with $R = 3$ and J varying from 0.2 to 0.45. This range of J encompasses the KH–Holmboe transition, which occurs at $J_{KH} = 0.261$. Note that the steering levels for modes with $J \geq 0.27$ are displaced from $z = 0$, which indicates that they are Holmboe modes. Each curve is labeled with the associated values of J and Ri_c, the latter being the gradient Richardson number at the steering level.

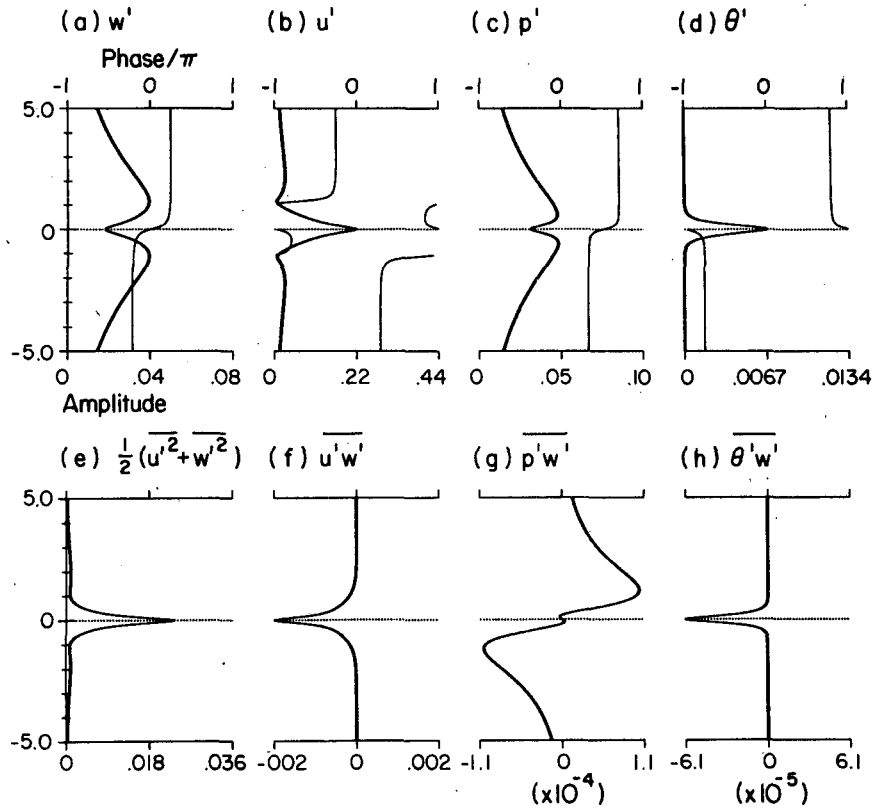

FIG. 11. Eigenfunctions and correlations for the faster-growing Kelvin–Helmholtz mode located close to the KH–Holmboe transition, illustrating energy trapping near critical level. Parameter values are $R = 3$, $J = 0.26$ and $\alpha = 0.3$.

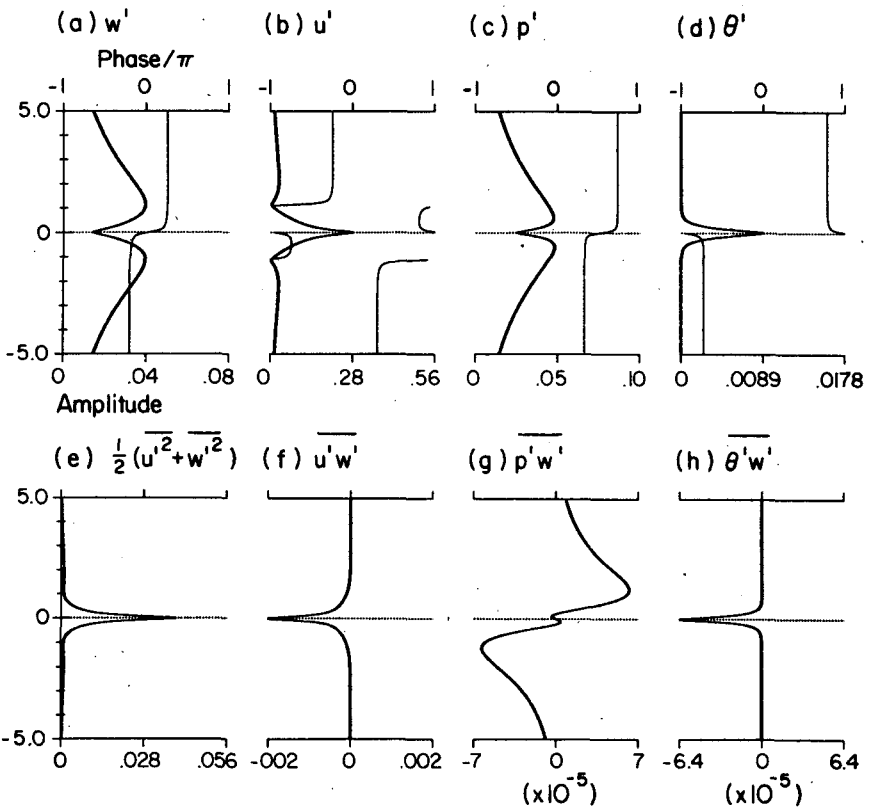

FIG. 12. Eigenfunctions for the slow-growing mode corresponding to the mode shown in Fig. 11.

The $J = 0.26$ curve corresponds to Fig. 13g. For $J < 0.25$, the flux divergence $d(\overline{p'w'})/dz$ at $z = 0$ is positive, and it decreases with increasing J. At $J = 0.25$, $d(\overline{p'w'})/dz$ at $z = 0$ vanishes. The energy sink surrounding $z = 0$ develops as J is increased beyond the value 0.25. As J is increased beyond $J_{KH} = 0.261$, the energy sink at $z = 0$ remains, but the steering level moves away from $z = 0$ and towards the outer regions of the shear layer, where $\mathrm{Ri}(z) < \frac{1}{4}$. When J reaches the value 0.29, we see that (i) the steering level reaches the upper boundary of the energy sink and (ii) the value of Ri_c drops below $\frac{1}{4}$. For $J > 0.29$, we have the situation shown in Figs. 7 and 8, in which the energy sink surrounding $z = 0$ exists but does not enclose the steering level. This calculation has been repeated with $\alpha = 0.6$, at which wavenumber the KH–Holmboe transition occurs at a value of J less than $\frac{1}{4}$, and it is found that the kink in the flux divergence at $z = 0$ does not develop. We thus conclude that the energy sink surrounding the steering level is a characteristic of flows for which the gradient Richardson number at the steering level exceeds $\frac{1}{4}$.

In addition to this anomalous spatial structure, unstable modes for which $\mathrm{Ri}_c > \frac{1}{4}$ exhibit relatively low growth rates (see Figs. 4a and 4b), and we suspect that these two properties may be causally linked, although the nature of that link is unclear at present. In a subsequent paper, we will explore the possibility that a normal mode may avoid exhibiting an energy sink near the steering level by propagating at an angle to the background flow. This could lead to three-dimensional normal modes having larger growth rates than their two-dimensional counterparts, in accordance with the predictions made by Lawrence et al. (1987) on the basis of Squire's theorem (Squire 1933; Yih 1955). Our results indicate that this can occur, but only in viscous flows (SKP; Smyth and Peltier 1990).

3. Overreflection analyses

Solutions of the Taylor–Goldstein equation may be constructed in one of two ways. If radiation/boundedness conditions (see section 2) are applied at both the upper and lower boundaries, the result is an eigenvalue problem which, for a given value of the wavenumber α, has solutions only if the phase speed c takes one of a discrete set of values. The eigenvalues c are in general complex, and a positive value of c_i indicates an exponentially growing eigenmode.

A second application of the Taylor–Goldstein equation, and one that we shall pursue in this section, is in the analysis of neutrally propagating internal waves. For this application we require that c be purely real or, more precisely, that c_i approach zero through positive values (e.g., Lindzen and Rosenthal 1983). When the value of c is restricted in this way, it is not generally possible to satisfy boundedness conditions at both the upper and lower boundaries. To describe internal waves incident upon the shear layer from below, for example, we impose a condition of upgoing radiation (i.e., transmitted waves only) at the upper boundary $z \to +\infty$, and allow the solution far below the shear layer to be composed of both upgoing (incident) and downgoing (reflected) waves. If the downgoing component

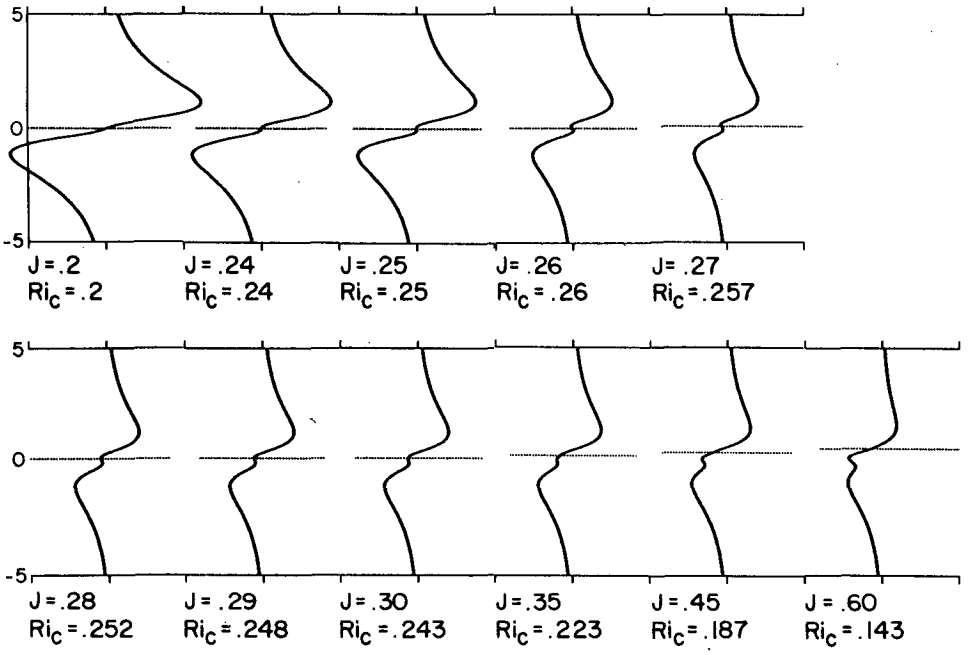

FIG. 13. $\overline{p'w'}$ profiles for $R = 3$, $\alpha = 0.3$, and J values indicated, showing that energy trapping near the critical level is a characteristic of modes for which $\mathrm{Ri}_c > \frac{1}{4}$.

of the solution has greater amplitude than the upgoing component, we conclude that the incident wavetrain is overreflected from the shear layer.

a. Qualitative overreflection analysis

If, somewhere below the shear layer, a region exists in which the refractive index

$$Q(z) = \frac{N^2}{(U-c)^2} - \frac{d^2U/dz^2}{U-c} - \alpha^2 \qquad (6)$$

is positive and approximately constant, then the reflection coefficient for waves incident on the shear layer from below may be calculated explicitly by employing the WKB method to resolve the solution into its upgoing and downgoing components and then computing the ratio of the amplitudes of those components (e.g., Davis and Peltier 1976, 1977). For the velocity and stratification profiles employed in this paper, no such region exists, but it is nonetheless possible to determine whether or not a given wavetrain is overreflected. We simply calculate the profile of the net energy flux $\overline{p'w'}$, exactly as was done in section 2, and note the sign of $\overline{p'w'}$ far below the shear layer. If $\overline{p'w'} < 0$ in this region, then the net energy flux is directed downward and we conclude that the reflected wave has greater amplitude than the incident wave, i.e., that the incident wave is overreflected. This connection between the sign of $\overline{p'w'}$ and the existence or nonexistence of overreflection has been established rigorously by Lindzen and Tung (1978). If the overreflected wavetrain is contained in some way, e.g., by a solid lower boundary or a turning point at some distance below the shear layer, then successive overreflections may cause the wavetrain to evolve into an exponentially growing disturbance (e.g., Lindzen 1974; Davis and Peltier 1977).

In discussing the overreflection mechanism, it is useful to define, for an unstable normal mode with given values for the parameters α and c, the "associated" neutral wave. This is the disturbance obtained by leaving α and c_r unchanged and taking the limit $c_i \to 0_+$. If the neutral wave associated with a given unstable normal mode is overreflected, then we may reasonably suspect that the overreflection mechanism is intimately related to the instability. Lindzen (personal communication, see also Lindzen and Rosenthal 1981) has suggested that an unstable normal mode might more usefully be identified with a stable wave field having a phase speed different from its own. Subject to this caveat, to which we will return in our concluding remarks, we will proceed here on the assumption that the phase speed of the overreflected wave field must match that of the unstable normal mode.

A simple modification to the numerical algorithm described in section 2 allows us to calculate $\overline{p'w'}$ in the region below the shear layer for the neutral wave field described above. We begin the integration of the Taylor–Goldstein equation at a large positive value of z, so that $Q(z)$ is nearly constant, and apply the boundary condition $d\psi'/dz = -\alpha\psi'$, just as was done in the linear stability analysis. This boundary condition is equivalent to the requirement of a positive vertical energy flux, as was discussed in section 2. We now integrate downward through the shear layer until we reach the half-space below the shear layer in which $Q(z)$ is constant. During this integration, c_i is set to a very small positive value that approximates the limit $c_i \to 0_+$. Finally, we calculate the profile of the net energy flux and use its sign to determine whether or not the neutral wavetrain is overreflected, as was discussed earlier in this section.

We shall now examine the energy flux profiles associated with some of the unstable modes whose spatial structures were investigated in section 2. In Fig. 14a, we show the $\overline{p'w'}$ profile for the neutral wave corresponding to the Kelvin–Helmholtz mode illustrated in Fig. 5. This profile reveals that the upgoing neutral wave is overreflected, since the net vertical energy flux below the critical level is negative. It is thus reasonable to suppose that overreflection is intimately related to for this instability. In Fig. 14b, we show the $\overline{p'w'}$ profile for the neutral wave corresponding to the Holmboe mode shown in Fig. 7. Once again we see, from the fact that $\overline{p'w'} < 0$ below the critical level, that the neutral wave is overreflected.

We now examine the neutral wave associated with an unstable normal mode that is located near the KH–Holmboe transition. In section 5, we plotted the eigenfunctions for a Kelvin–Helmholtz mode with J slightly less than the transition value J_{KH} (see Figs. 11 and 12). For the qualitative overreflection analysis in the transition region, we examine a Holmboe mode growing on a background flow with J slightly greater than J_{KH}. Specifically, we choose $R = 3$, $J = 0.28$, and $\alpha = 0.3$. These parameter values deliver a complex conjugate pair of Holmboe modes with $c = \pm 0.085219 + 0.108708i$. The $\overline{p'w'}$ correlations for the neutral waves associated with the right-going and left-going Holmboe modes are shown in Figs. 14c and 14d, respectively. Since Ri_c exceeds ¼ in this case, we do not expect the neutral waves to be overreflected. The $\overline{p'w'}$ profiles in Figs. 14c and 14d confirm this by showing that the net vertical energy flux below the critical level is positive in each case. These results suggest that instability may not always be intimately related to overreflection.

b. Quantitative overreflection analysis: methodology

We have seen how quantitative information regarding the existence or nonexistence of overreflection may be obtained by examining the $\overline{p'w'}$ profile for a neutrally propagating wavetrain. This approach has confirmed that neutral waves whose critical layers lie in the region where $\mathrm{Ri} > ¼$ are not overreflected, even though they are related to growing normal modes. We now turn to the explicit calculation of reflection coef-

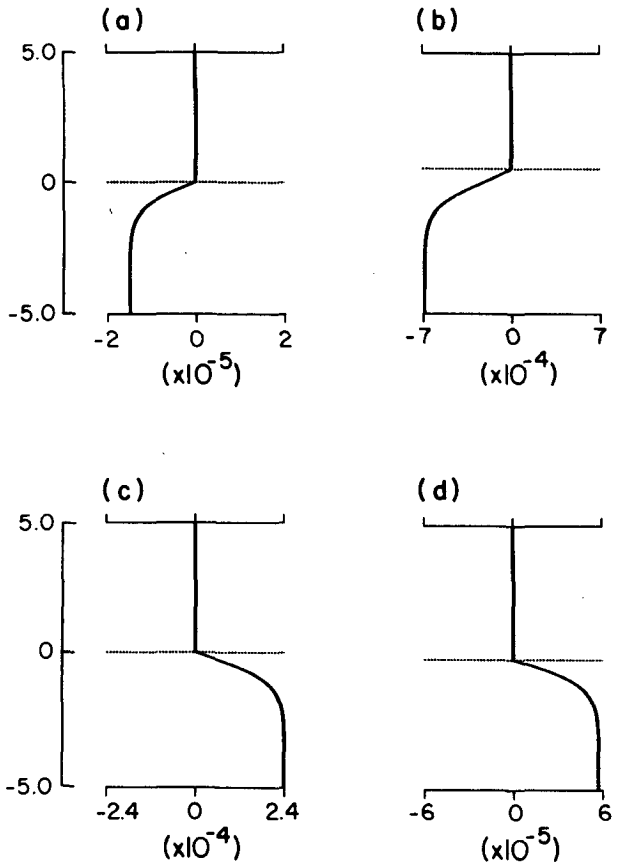

FIG. 14. $\overline{p'w'}$ profiles for (a) the overreflected neutral wave corresponding to the unstable Kelvin–Helmholtz mode shown in Fig. 5, $c_i = 0.0001$; (b) the overreflected neutral wave corresponding to the unstable Holmboe mode shown in Fig. 7, $c_i = 0.0001$; (c) the neutral wavetrain with $\alpha = 0.3$, $c_r = 0.0852$, $c_i = 0.0001$, on a flow with $R = 3$ and $J = 0.28$ (the wavetrain is not overreflected); (d) same as (c), except that $c_r = -0.0852$.

ficients for neutral waves incident on a shear layer. In these calculations, we shall follow closely the methodology of Lindzen and Rosenthal (1983, hereafter referred to as LR) so that our results for the general Kelvin–Helmholtz–Holmboe flows may be compared to their results for the Kelvin–Helmholtz case.

The background profiles of velocity and Brunt–Väisälä frequency to be employed in these analyses have been chosen as follows. We employ a velocity profile that approximates the piecewise-linear shear layer:

$$U(z) = \begin{cases} 1, & \text{if } z > 1 \\ z, & \text{if } -1 < z < 1 \\ -1, & \text{if } z < -1, \end{cases} \tag{7}$$

although minor modifications (to be described below) are made to facilitate the calculation of reflection coefficients. As in the calculations described in previous sections, the Brunt–Väisälä frequency profile is given by (2). We investigate three separate classes of flows, characterized by scale ratios $R = 0$, $R = 1$ and $R = 3$, choosing various values of J in each case. These analyses constitute an extension of the work of LR, who investigated the case $R = 0$, $J = 0.15$. We shall begin with a discussion of the modifications to (7) which are necessary in order that we may calculate reflection coefficients explicitly.

Reflection analysis is only feasible if the index of refraction $Q(z)$ is positive in some region of the domain and varies slowly enough to satisfy the WKB criterion

$$\frac{|dQ/dz|}{|Q^{3/2}|} \ll 1, \tag{8}$$

in order that the solution in that region may be represented as a superposition of oppositely propagating waves by means of the WKB approximation. Furthermore, such a region must be located between the critical level and some other reflecting region (e.g., a boundary or a turning point), so that successive overreflections may occur. We refer to such regions as "waveguides." If a waveguide does not exist in the flow we wish to examine, then it must be created artificially by modifying the background flow. If the necessary modifications can be made in such a way that the qualitative form and the stability characteristics of the flow are not significantly altered, then the results of the reflection analysis may be considered applicable to the original (unmodified) flow.

For example, in Davis and Peltier's (1976, 1977) model of overreflected gravity waves, a large region of constant, positive Q existed in which the reflection analysis could be performed, whereas in the work of Lindzen et al. (1980) concerning baroclinic instability, and in LR's study of Kelvin–Helmholtz instability, waveguides had to be created artificially. In the present work, the background velocity profile must be constructed deliberately in order that waveguides exist, and we will do so following the approach of LR.

The velocity profile (7) has discontinuities in dU/dz at $z = \pm 1$, so that the term involving d^2U/dz^2 in the refractive index is infinite at those points. If we can smooth the profile in the regions near $z = \pm 1$ in such a way that dU/dz is continuous, and that the term involving d^2U/dz^2 in $Q(z)$ is constant and much larger than the other terms in (6), then we will have waveguides in those regions. Accordingly, we replace (7) with a smoothed profile given by

$$U(z) = \begin{cases} 1 & \text{if } z > 1 + b' \\ U_1(z) & \text{if } 1 - a' < z < 1 + b' \\ z, & \text{if } -1 + a < z < 1 - a' \\ U_2(z) & \text{if } -1 - b < z < -1 + a \\ -1 & \text{if } z < -1 - b. \end{cases} \tag{9}$$

The constants a, b, a', and b' are to be determined by

continuity conditions. We require that the functions $U_1(z)$ and $U_2(z)$ obey the equation

$$\frac{d^2U/dz^2}{U-c} = -\mu^2, \tag{10}$$

in which μ^2 is a constant chosen large enough that the refractive index may be approximated accurately by $Q(z) = \mu^2$, i.e., large enough that (8) is satisfied. Equation (10) has solutions

$$U_1(z) = c_r + \frac{1}{\mu}\sin\mu(z-1+a') + (1-a'-c_r)\cos\mu(z-1+a'), \tag{11a}$$

$$U_2(z) = c_r + \frac{1}{\mu}\sin\mu(z+1-a) + (-1+a-c_r)\cos\mu(z+1-a), \tag{11b}$$

which satisfy the conditions that U and dU/dz be continuous at $z = 1 - a'$ and $z = -1 + a$. The remaining four continuity conditions deliver a set of four nonlinear algebraic equations for the waveguide limits a, b, a', and b', namely:

$$-1 = c_r - \frac{1}{\mu}\sin\mu(a+b) + (-1+a-c_r)\cos\mu(a+b) \tag{12a}$$

$$0 = \cos\mu(a+b) + (-1+a-c_r)\mu\sin\mu(a+b) \tag{12b}$$

$$1 = c_r + \frac{1}{\mu}\sin\mu(a'+b') + (1-a'-c_r)\cos\mu(a'+b') \tag{12c}$$

$$0 = \cos\mu(a'+b') - (1-a'-c_r)\mu\sin\mu(a'+b'). \tag{12d}$$

For the numerical calculations to be reported here, we solve (12) using a high-precision iterative algorithm.

Note that the velocity profile (9) now depends upon the horizontal phase speed c_r of the disturbance. This is not a problem provided that μ is large, for then the dependence of $U(z)$ on c_r, and its effect on the stability characteristics of the flow, are negligible. Choosing a sufficiently large value for μ also ensures that (8) is satisfied. In the analyses to be discussed here, we set $\mu = 20$.

Sample profiles of the vertical wavenumber $\sqrt{Q(z)}$, computed using the velocity profile (9) and the stratification profile (2) with various choices of parameter values, are shown in Fig. 15. The first two plots correspond to Kelvin–Helmholtz modes, with steering levels located at $z = 0$. The third and fourth plots correspond to Holmboe modes. (The value $\mu = 20$ that is employed in the quantitative overreflection calculations delivers waveguides that are very long in the $\sqrt{Q}$ direction and thin in the z direction, which makes the $\sqrt{Q}$ profiles very difficult to plot; we have reduced the value of μ to 10 in the construction of Fig. 15 for this reason.)

We turn now to the calculation of the reflection coefficients for neutral waves propagating on a background flow with $U(z)$ given by (9) and $N^2(z)$ given by (2). We will deal first with the upper waveguide. Suppose that we allow c to have a positive imaginary part. If μ is sufficiently large, (8) is still satisfied and we may consider $Q(z)$ to be constant in the waveguide, in which case we may write:

$$Q(z) \approx Q(z_0) = m^2, \tag{13}$$

in which m is a complex constant chosen so that $m_r > 0$ and $m_i \leq 0$. If $c_i = 0$, then $m = \mu$. The solution of (3) in the upper waveguide is then given by

$$\psi' = Ae^{imz} + Be^{-imz}, \tag{14}$$

in which A and B are complex constants. In the limit $c_i \to 0_+$, it is easily shown (Booker and Bretherton 1967) that the first term on the rhs of (14) has associated with it a vertical energy flux whose sign is the same as that of $U - c_r$. It may be shown in a similar manner that the sign of the energy flux associated with the second term on the rhs of (14) is opposite to that of $U - c_r$. Since $U - c_r > 0$ in the upper waveguide, the terms on the rhs of (14) represent an upgoing wave and a downgoing wave, respectively.

Reflection coefficients are calculated by examining numerical solutions of (3), applying the appropriate boundary conditions in each case. To find the complex reflection coefficient for a downgoing wave reflected from the region below the upper waveguide, we integrate (3) upward from a large negative value of z, at which an outgoing radiation condition is applied. We stop the integration at $z = z_0 - a'$ (the bottom of the upper waveguide), and determine values $A = A_-$ and $B = B_-$ for the constants in (14), by requiring continuity of the solution ψ' and its derivative. The reflection coefficient is then given by the ratio of the first term on the rhs of (14) to the second term on the rhs of (14), evaluated at the top of the waveguide, viz.:

$$R = R_- e^{2im(z_0-a')},$$

in which $R_- = A_-/B_-$. If $|R| > 1$, then the downgoing waves are overreflected.

To find the reflection coefficient for upgoing waves reflected from the region above the upper waveguide, we reverse the procedure just described. We apply an outgoing radiation condition at a large positive value of z, integrate downward to the top of the upper waveguide, and match the solution to (14) to obtain values $A = A_+$ and $B = B_+$ for the constants. The reflection coefficient is now given by

$$R = R_+ e^{-2im(z_0+b')},$$

in which $R_+ = B_+/A_+$.

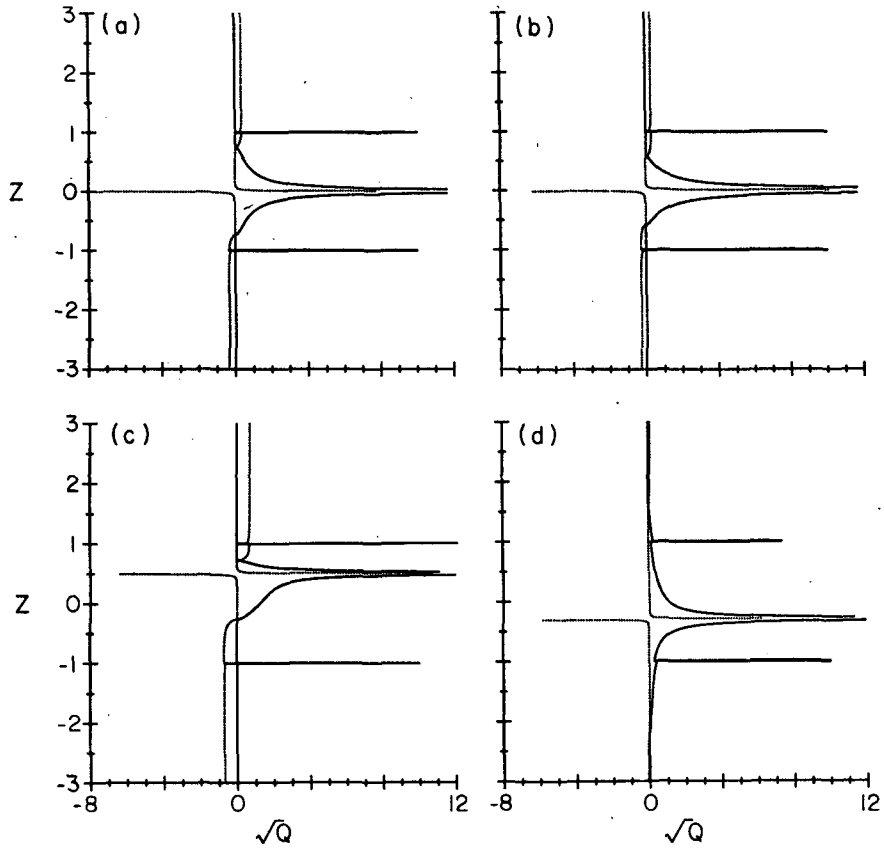

FIG. 15. Profiles of vertical wavenumber $\sqrt{Q(z)}$. Parameter values are: (a) $R = 0$, $J = 0.15$, $\alpha = 0.523$, $c_r = 0$; (b) $R = 3$, $J = 0.26$, $\alpha = 0.3$, $c_r = 0$; (c) $R = 3$, $J = 0.5$, $\alpha = 0.7$, $c_r = 0.51$; (d) $R = 1$, $J = 0.1$, $\alpha = 0.1$, $c_r = -0.3$. In each case, $\mu = 10$ and $c_i = 0.001$. Solid curves indicate the real part of $\sqrt{Q}$; dotted curves indicate the imaginary part.

When the two reflection processes described above occur in succession, the total reflection coefficient is

$$R_T = R_+ R_- e^{-2im(a'+b')}. \tag{15}$$

The numerical integrations involved in the computation of R_T are performed as before using the ODE solver ERNY. A first-order Frobenius series solution of the Taylor–Goldstein equation (for details see Miles 1961) is employed to bypass singularities which arise in the limit $c_i \to 0_+$.

For the quantization condition to be satisfied, the upgoing waves A_+e^{imz} and A_-e^{imz} must be in phase, and likewise the downgoing waves B_+e^{-imz} and B_-e^{-imz}. These conditions are equivalent to the requirements that the constants A_+/A_- and B_+/B_- be real and positive. Solutions of (3) are determined only up to a multiplicative constant, and we can choose that constant so that one of the above conditions is satisfied. In order that both conditions be satisfied, we must require that the quotient $(B_+/B_-)/(A_+/A_-)$, which is equal to R_+R_-, be real and positive. Thus, the quantization condition may be expressed as

$$(R_+R_-)_r > 0, \quad (R_+R_-)_i = 0. \tag{16}$$

For future reference, we note that the two solutions of the Taylor–Goldstein equation (3) which have the WKB forms $A_+e^{imz} + B_+e^{-imz}$ and $A_-e^{imz} + B_-e^{-imz}$ inside the upper waveguide may be matched to create a continuous solution of (3), having continuous derivative and satisfying both upper and lower boundary conditions, if and only if the WKB expressions just given are equal throughout the waveguide, i.e., if $A_+ = A_-$ and $B_+ = B_-$. The matching condition which defines normal modes in the usual stability problem may thus be defined as

$$R_+R_- = 1. \tag{17}$$

In the lower waveguide, the analysis goes exactly as above, except that the interpretation of the terms on the rhs of (14) as upgoing and downgoing waves is reversed, because $U - c_r < 0$ in that region.

c. *Quantitative overreflection analysis: results*

In Fig. 16, we compare the phase speeds predicted by linear stability analysis and resonant overreflection theory, plotting phase speed versus wavenumber for several values of R and J. The solid curves indicate

the predictions of linear stability analysis. The predictions of overreflection theory, computed at selected values of α in the manner described above, are shown by circles and crosses, which indicate modes overreflected in the upper and lower waveguides, respectively.

Figure 16 illustrates clearly the difficulty of understanding the stability properties of these flows based on the reflection characteristics of neutral internal waves. Exceptions to this occur in the Holmboe wave regime well away from the KH–Holmboe transition, where phase speeds are predicted accurately. For example, in Figs. 16e and 16f the phase speeds predicted by the two theories become equal at large values of α. Good agreement is also found at small values of α in Figs. 16a, 16e and 16f, although in those regions overreflection theory also delivers spurious normal mode instabilities that are not predicted by linear stability analysis.

In Figs. 16a, 16b and 16c, we see that the right-hand (large α) stability boundary is not well predicted by overreflection theory. In Fig. 16a, for example, overreflection theory predicts unstable normal modes at $\alpha = 0.7$, even though the stability boundary is located at $\alpha = 0.64$ according to linear stability analysis.

We have computed reflection coefficients at a large number of points on the α–J plane for the cases $R = 0$, $R = 1$ and $R = 3$, in order to identify the regions of parameter space in which the predictions of resonant

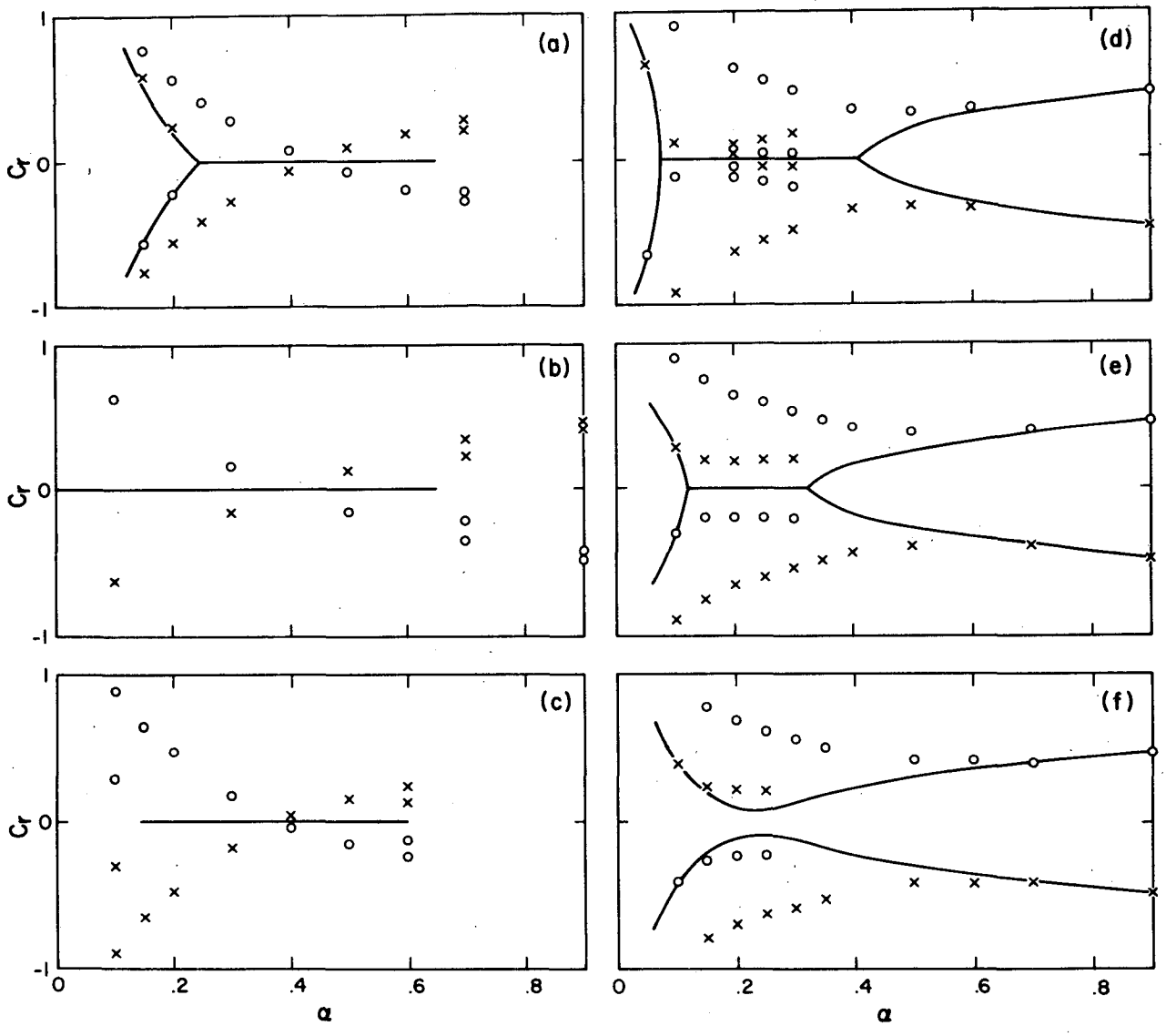

FIG. 16. Horizontal phase speed versus wavenumber. Solid curves illustrate predictions of linear stability analysis; symbols indicate growing modes predicted by overreflection theory. Crosses and circles represent modes overreflected in the upper and lower waveguides, respectively. Parameter values are: (a) $R = 0$, $J = 0.05$; (b) $R = 1$, $J = 0.01$; (c) $R = 1$, $J = 0.1$; (d) $R = 3$, $J = 0.2$; (e) $R = 3$, $J = 0.26$; (f) $R = 3$, $J = 0.3$.

overreflection theory agree and disagree with those of linear stability analysis. The results are summarized in Fig. 17. In these plots, the curves represent results from linear stability analysis. Solid curves indicate stability boundaries, dashed curves represent KH–Holmboe transitions (with the symbols KH and H designating the type of instability found on each side of the transition), and dotted curves represent the loci of the fastest-growing modes, i.e., the curves upon which $\sigma_r = \sigma_r(\alpha)$ for fixed J is a maximum. Note that the c_r versus α plots shown in Fig. 5 correspond to horizontal cross sections of the plots shown in Fig. 16. The locations of the cross sections to which Figs. 16a through 16f correspond are labeled with the numerals 1 through 6, respectively.

Before looking at the results from overreflection theory (shown by crosses and circles), we will examine briefly the qualitative stability characteristics of these flows. Figure 17a reveals the interesting result that Holmboe instability is possible in a flow with constant stratification (i.e., with $R = 0$). This refutes the common belief that Holmboe instability arises only when a strong concentration of stratification is near the center of the shear layer. This result is also evident in the work of Rosenthal and Lindzen (1983), although the Holmboe modes are not identified as such in that paper. The qualitative stability characteristics for the $R = 1$ case (Fig. 17b) closely resemble those of the corresponding hyperbolic tangent shear layer (cf. Fig. 4d). In that case, the stability boundary is given by the parabola $J = \alpha(1 - \alpha)$ (Holmboe 1962). The $R = 3$ case (Fig. 17c) differs from its hyperbolic tangent counterpart (cf. Fig. 4b) primarily in the region of large α and small J. We find that the piecewise-linear shear layer with $R = 3$ is unstable for arbitrarily large α, provided that J is nonzero. A similar result has been established by Nishida and Yoshida (1984) for the case of a hyperbolic tangent shear layer in the limit $R \to \infty$.

The crosses and circles in Fig. 17 indicate the predictions of resonant overreflection theory, based on the overreflection of neutral modes, for comparison with those of linear stability analysis. They are interpreted as follows:

(i) Blank circle: Both theories predict instability, and the absolute value of the difference in the predicted horizontal phase speeds does not exceed 0.1. (LR encountered discrepancies having magnitudes of up to 0.07 in the predicted value of c_r, and did not consider them worthy of comment. In interpreting our results, we have accepted this implicit error tolerance and have increased it, for simplicity, to the value 0.1.)

(ii) Half-shaded circle: Both theories predict instability, but the absolute difference in predicted phase speeds exceeds 0.1. If resonant overreflection theory gives more than one value for c_r, we consider only the value which agrees most closely with the prediction of linear stability analysis. If the right half-circle is shaded, the phase speed predicted by resonant overreflection theory in the upper waveguide is greater than the phase speed predicted by linear stability analysis. If the left half-circle is shaded, the reverse is true. If the circle is enclosed within a larger circle, then the neutral wave associated with the unstable mode predicted by linear stability analysis (i.e., having the same phase speed) is not overreflected.

(iii) Fully shaded circle: Resonant overreflection theory predicts one or more unstable modes, even though linear stability analysis shows that the flow is stable.

(iv) Cross: Resonant overreflection theory does not predict any instability. In all such cases, we have found that linear stability analysis also shows the flow to be stable.

For the most part, the predictions of overreflection theory regarding the stability or instability of the flow are in accord with those of linear stability analysis; however, there are several points at which overreflection theory predicts instability even though the flow is stable according to linear stability analysis, as was noted in the discussion of Fig. 16.

There are large regions of parameter space in which resonant overreflection theory fails to predict the value of c_r to within the tolerance 0.1. It should be noted, however, that the phase speeds of the fastest-growing modes are predicted accurately. For wavenumbers smaller than that of the fastest-growing mode, the phase speed predicted in the upper waveguide is generally less than that given by linear stability analysis. For wavenumbers larger than that of the fastest-growing mode, the reverse is true. This result is also evident in Fig. 6 of LR.

In the case $R = 0$, the Holmboe modes which exist at small α are predicted accurately by resonant overreflection theory. In the case $R = 3$, the Holmboe modes found at large α are predicted accurately. The Holmboe modes which occur at small α in this case are also well predicted, but the quantization condition is satisfied at more than one value of c_r for most of these modes and, as was mentioned earlier, we choose the value of c_r which agrees best with the prediction of linear stability analysis.

The double circles in Fig. 17c indicate points at which normal modes are unstable even though their associated neutral waves are not overreflected. This phenomenon occurs in a region which surrounds the KH–Holmboe transition and which is thickest at large values of J and thinnest at small values of J. In particular, the phenomenon occurs whenever the critical level for the associated neutral wave is located in a region where the gradient Richardson number exceeds ¼.

d. Additional aspects of overreflection analysis

Lindzen and Rosenthal (1983) showed that discrepancies between the predictions of overreflection theory

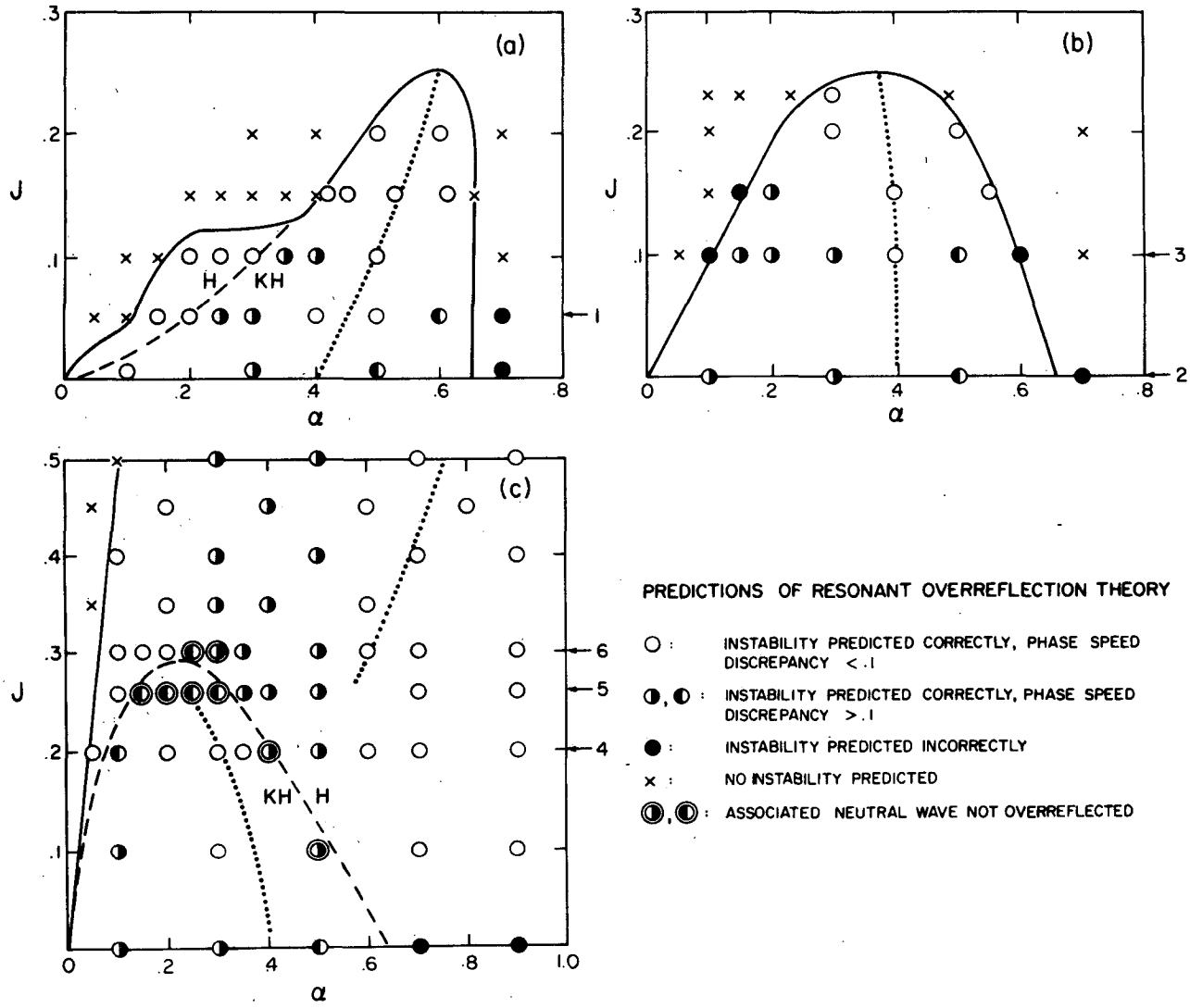

FIG. 17. Accuracy of predictions based on overreflection theory. Symbols defined in the legend are overlaid on stability diagrams generated by linear stability analysis. Solid curves represent stability boundaries, dotted curves indicate the fastest-growing mode at each J, and dashed curves show the KH–Holmboe transition. Cross sections corresponding to Figs. 16a–f are indicated by arrows numbered 1 to 6, respectively. Parameter values are: (a) $R = 0$, (b) $R = 1$ and (c) $R = 3$.

and those of linear stability analysis may be removed via a consideration of the necessity that there exist a balance between the time scale upon which overreflection develops (Lindzen and Barker 1985) and the time scale upon which the resulting disturbance is predicted to grow. LR found that this balance could in general only be achieved by computing the reflection coefficient using a nonzero value for the imaginary part of the phase speed. [This procedure is justified in part by a result of Lindzen and Rosenthal (1981), in which it is shown that unstable normal modes may be considered as analytic continuations of overreflected neutral waves.] LR stated that a reflection coefficient calculated using a nonzero value of c_i corresponds to the amount of overreflection that develops on a time scale $\tau = 1/\alpha c_i$ (i.e., the e-folding time associated with c_i), and showed, based on this assumption, that the aforementioned time scales are mutually consistent only if the value of c_i predicted using overreflection theory is equal to the value of c_i employed in calculating the reflection coefficient. Using our notation, this condition is expressed mathematically as

$$c_{i,\text{pred}} = \frac{\ln|R_+R_-e^{-2m_i(a'+b')}|}{2\alpha T} = c_i, \qquad (18)$$

in which m_i is the imaginary part of m [see (13)] and T is the time required for the propagating disturbance

to traverse the waveguide.[2] In addition to the consistency condition (18), it is required that c_r be such that the quantization condition is satisfied.

Lindzen and Rosenthal (1983) employed an iteration scheme equivalent to Newton's method in order to find the value of c which would satisfy the above conditions, and showed, at selected points in parameter space, that the resulting value of c agreed well with the value predicted using linear stability analysis. We could carry out the same procedure here, but we find it to be unnecessary, as it may readily be shown that (18), in combination with the quantization condition (16), is equivalent to the matching condition which defines normal modes of the stability equation. To see this, we note first that the travel time T may be expressed as $(a' + b')m_i/\alpha c_i$ (see LR), and use this result to rewrite (18) as

$$c_{i,\text{pred}} = \frac{\ln|R_+R_-|}{2\alpha T} + c_i = c_i.$$

This equation clearly is satisfied if and only if $|R_+R_-| = 1$. Recalling that the quantization condition requires R_+R_- to be real and positive, we conclude that the consistency condition (18) is equivalent to $R_+R_- = 1$, which is just the matching condition (17) for the stability problem. Thus the iteration scheme devised by LR must converge *exactly* to the phase speed predicted by linear stability analysis at *every* point in parameter space.

Although the considerations described above formally remove the discrepancies between the predictions of overreflection theory and those of linear stability analysis that were noted in the preceding section, the physical meaning of the result is not at all clear, as discussed in section 4 of this paper.

4. Discussion

We believe that the most useful purpose that overreflection theory could serve would be to provide a clear, physical picture of the manner in which normal mode instabilities of a dynamical origin actively develop. The initial disturbance is assumed to consist of small amplitude neutral waves which, through repeated overreflection, develop into a growing normal mode (e.g., Lindzen 1974; Davis and Peltier 1976; Pellacani et al. 1979; Lindzen et al. 1980; LR; Lindzen and Barker 1985; Lindzen 1988).

It is apparent in our results and in the results of numerous previous studies that a large region of parameter space exists in which the neutral wave having the same horizontal wavenumber and phase speed as the most unstable normal mode is overreflected and obeys the quantization condition. In this case, it is easy to imagine that the mechanism described above is responsible for the instability, and that the consistency condition (18) might reasonably be employed in order to correct the overestimation of the growth rate which results when the reflection coefficient is calculated for the limit $c_i \to 0_+$.

We have shown, however, that a substantial region of parameter space also exists in which the neutral mode having the same horizontal wavenumber and phase speed as the most unstable mode does not obey the quantization condition. Furthermore, we have shown that, near the KH–Holmboe transition, this neutral mode is not overreflected. If unstable normal modes existing in these regions of parameter space are to be viewed as arising from overreflected internal waves, then those waves that are overreflected initially must have wavenumbers and/or phase speeds that do not match those of the unstable modes.

The intriguing result which has been established numerically by LR and proven analytically in the present paper, namely that shear flow instabilities may always be identified with overreflected waves provided that LR's consistency condition (18) is employed, suggests strongly that the anomalies which we have encountered here are formally resolvable. However, the manner in which a confined, overreflected, linear wave field might exhibit a change in its phase speed and/or its wavenumber as it develops into a growing normal mode is not at all obvious. For this reason, the results presented here lead us to suggest that further research is needed in order to clarify the relationship between shear flow instability and overreflection. It is our hope that these results will serve to motivate continued study in this area.

The analyses presented in this paper are part of an ongoing investigation of the unique physical properties exhibited by unstable normal modes located in the vicinity of the KH–Holmboe transition. In section 2d, we showed that modes located in this area of parameter space are characterized by an anomalous spatial structure that causes the region surrounding the steering level to act as an energy sink for the disturbance, despite the fact that energy is transferred from the background shear in this region via the Reynolds stress. In the context of overreflection, this unusual property is manifested in the existence of unstable normal modes that are not correlated with overreflected neutral waves. In a subsequent paper, we will show that including viscosity and heat conduction in the model may lead to preferential destabilization of obliquely propagating Holmboe modes in this region of parameter space, thus allowing a direct transition to three-dimensional flow without the need for an intervening two-dimensional state.

[2] The first equality of (18) is equivalent to the first unnumbered equation given in the Appendix of LR. The "c_i" which appears in the second equality of (18) is LR's "$(c_i)_{\text{orig}}$." The minus sign in the exponent reflects the fact that we are considering a waveguide which is located at the top of the shear layer, whereas LR's waveguide was located near the bottom of the shear layer.

Acknowledgments. The research reported in this paper was supported by the Natural Sciences and Engineering Research Council of Canada, under Grant A9627 and by a grant from the Atmospheric Environment Service of Canada.

REFERENCES

Booker, J. R., and F. P. Bretherton, 1967: The critical layer for internal gravity waves in a shear flow. *J. Fluid Mech.*, **27**, 513–539.

Browand, F. K., and C. D. Winant, 1973: Laboratory observations of shear instability in a stratified fluid. *Bound-Layer Meteor.*, **5**, 67–77.

Davis, P. A., and W. R. Peltier, 1976: Resonant parallel shear instability in the stably stratified planetary boundary layer. *J. Atmos. Sci.*, **33**, 1287–1300.

——, and ——, 1977: Effects of dissipation on parallel shear instability near the ground. *J. Atmos. Sci.*, **34**, 1868–1884.

Ellison, T. H., and J. S. Turner, 1959: Turbulent entrainment in stratified flows. *J. Fluid Mech.*, **6**, 423–440.

Hazel, P., 1972: Numerical studies of the stability of inviscid parallel shear flows. *J. Fluid. Mech.*, **51**, 39–62.

Holmboe, J., 1962: On the behavior of symmetric waves in stratified shear layers. *Geophys. Publ.*, **24**, 67–113.

Howard, L. N., 1961: Note on a paper of John W. Miles. *J. Fluid Mech.*, **10**, 509–512.

Jones, W. L., 1968: Reflexion and stability of waves in stably stratified fluids with shear flow: A numerical study. *J. Fluid Mech.*, **34**, 609–624.

Keulegan, G. H., 1949: Interfacial instabilities and mixing in stratified flows. *J. Res. Natl. Bur. Stand.*, **43**, 487–499.

Klaassen, G. K., and W. R. Peltier, 1985: The evolution of finite amplitude Kelvin–Helmholtz billows in two spatial dimensions. *J. Atmos. Sci.*, **42**, 1321–1339.

Koop, C. G., and F. K. Browand, 1979: Instability and turbulence in a stratified layer with shear. *J. Fluid Mech.*, **93**, 135–159.

Lawrence, G. A., J. C. Lasheras and F. K. Browand, 1987: Shear instabilities in stratified flow. *Proc. Third International Symposium on Stratified Flows*, Pasadena.

Lindzen, R. S., 1974: Stability of a Helmholtz velocity profile in a continuously stratified infinite Boussinesq fluid-applications to clear air turbulence. *J. Atmos. Sci.*, **31**, 1507–1514.

——, 1988: Instability of plane parallel shear flow (Toward a mechanistic picture of how it works). PAGEOPH, 126, 103–121.

——, and K. K. Tung, 1978: Wave overreflection and shear instability. *J. Atmos. Sci.*, **35**, 1626–1632.

——, and A. J. Rosenthal, 1981: A WKB analysis of baroclinic instability. *J. Atmos. Sci.*, **38**, 619–629.

——, and ——, 1983: Instability in a stratified fluid having one critical level. Part III: Kelvin–Helmholtz instabilities as overreflected waves. *J. Atmos. Sci.*, **40**, 530–542.

——, and J. W. Barker, 1985: Instability and wave overreflection in stably stratified flow. *J. Fluid Mech.*, **151**, 189–217.

——, B. Farrell and K. K. Tung, 1980: The concept of wave overreflection and its application to baroclinic instability. *J. Atmos. Sci.*, **37**, 44–63.

Maxworthy, T., and F. K. Browand, 1975: Experiments in rotating and stratified flows: Oceanographic applications. *Ann. Rev. Fluid Mech.*, **7**, 273–305.

Miles, J. W., 1961: On the stability of heterogeneous shear flows. *J. Fluid Mech.*, **10**, 496–508.

Muller, D. E., 1956: A method for solving algebraic equations using an automatic computer. *Mathematical Tables and Aids to Computation*, **10**, 208–215.

Nishida, S., and S. Yoshida, 1982: Stability of a two-layer shear flow. *Theor. Appl. Mech.*, **32**, 35–45.

Pellacani, C., C. Tebaldi and E. Tosi, 1979: Instabilities induced by over-reflection in stratified fluids in horizontal sheared motion. *Phys. Fluids*, **22**(4), 599–602.

Rosenthal, A. J., and R. S. Lindzen, 1983: Instabilities in a stratified fluid having one critical level. Part I: Results. *J. Atmos. Sci.*, **40**, 509–520.

Sharp, P. W., and J. M. Fine, 1987: User guide for ERNY: An explicit Runge-Kutta Nystrom integrator for second order initial value problems., University of Toronto Department of Computer Science, Technical Report #198. [May be obtained by writing to: Prof. P. Sharp, Dept. of Computer Science, University of Toronto, Toronto, Canada M5S 1A4.]

Smyth, W. D., and W. R. Peltier, 1990: Three dimensional instabilities of a stratified dissipative parallel flow. *Geophys. Astrophys. Fluid Dyn.*, in press.

——, G. P. Klaassen and W. R. Peltier, 1988: Finite amplitude Holmboe waves. *Geophys. Astrophys. Fluid Dynamics*, **43**, 181–222.

Squire, H. B., 1933: On the stability of three-dimensional disturbances of viscous flows between parallel walls. *Proc. Roy. Soc. London, A* **142**, 621–631.

Thorpe, S. A., 1968: A method of producing a shear flow in a stratified fluid. *J. Fluid Mech.*, **32**, 693–704.

Townsend, A. A., 1958: Turbulent flow in a stably stratified atmosphere. *J. Fluid Mech.*, **3**, 361–372.

Tritton, D. J., and P. A. Davies, 1985: Instabilities in geophysical fluid dynamics. *Hydrodynamic Instabilities and the Transition to Turbulence*, 2nd ed., H. L. Swinney and J. P. Gollub, Eds., Springer-Verlag.

Yih, C.-S., 1955: Stability of two-dimensional parallel flows for three-dimensional disturbances. *Q. Appl. Math.*, **12**, 434–435.

Yoshida, S., 1977: On a mechanism for breaking of interfacial waves. *Coastal Eng. Japan*, **20**, 7–15.